

Department of Physics, Chemistry and Biology

Master's Thesis

Search for Dark Matter in the Upgraded High Luminosity LHC at CERN

Impact of ATLAS phase II performance on a mono-jet analysis

Sven-Patrik Hallsjö

Thesis work performed at Stockholm University

Linköping, June 4, 2014

LITH-IFM-A-EX--14/2863--SE



**Linköpings universitet
TEKNISKA HÖGSKOLAN**

Department of Physics, Chemistry and Biology
Linköping University
SE-581 83 Linköping, Sweden

Search for Dark Matter in the Upgraded High Luminosity LHC at CERN

Impact of ATLAS phase II performance on a mono-jet analysis

Sven-Patrik Hallsjö

Thesis work performed at Stockholm University

Linköping, June 4, 2014

Supervisor: **Docent Christophe Clément**
 FYSIKUM Stockholm University
Professor Magnus Johansson
 IFM, Linköping University

Examiner: **Professor Magnus Johansson**
 IFM, Linköping University



Avdelning, Institution
Division, Department

Theoretical physics group
Department of Physics, Chemistry and Biology
SE-581 83 Linköping

Datum
Date

2014-06-04

Språk
Language

Svenska/Swedish
 Engelska/English

Rapporttyp
Report category

Licentiatavhandling
 Examensarbete
 C-uppsats
 D-uppsats
 Övrig rapport

ISBN
—

ISRN
LITH-IFM-A-EX--14/2863--SE

Serietitel och serienummer **ISSN**
Title of series, numbering —

URL för elektronisk version

<http://urn.kb.se/resolve?urn=urn:nbn:se:liu:diva-XXXXXX>

Titel Sökandet efter mörk materia i den uppgraderade hög luminositets LHC i CERN
Title Search for Dark Matter in the Upgraded High Luminosity LHC at CERN

Undertitel Påverkan av ATLAS fas II prestanda på en mono-jet analys
Subtitle Impact of ATLAS phase II performance on a mono-jet analysis

Författare Sven-Patrik Hallsjö
Author

Sammanfattning
Abstract

Disclaimer: Abstract not yet completed.

Something as an introduction:

The LHC at CERN is undergoing an upgrade to increase the center of mass energy for the colliding particles which means that new physical processes will be explored. One drawback of this is that it will be harder to isolate unique particle collisions since more and more collisions will occur simultaneously, so called pile-up.

One hope for the upgrade is that WIMP models of dark matter will be detected.

This thesis covers looking at effective operators which try to explain dark matter without adding new theories to the standard model or QFT.

Some results and a slight conclusion.

Nyckelord

Keywords

Disclaimer: This not yet completed., ATLAS, Beyond standard model physics, CERN, Dark matter, Elementary particle physics, High energy physics, something, this is in mythesis.sty

4 **Abstract**

5 **Disclaimer: Abstract not yet completed.**

6 Something as an introduction:

7 The LHC at CERN is undergoing an upgrade to increase the center of mass en-
8 ergy for the colliding particles which means that new physical processes will be
9 explored. One drawback of this is that it will be harder to isolate unique parti-
10 cle collisions since more and more collisions will occur simultaneously, so called
11 pile-up.

12 One hope for the upgrade is that WIMP models of dark matter will be detected.

13 This thesis covers looking at effective operators which try to explain dark matter
14 without adding new theories to the standard model or QFT.

15 Some results and a slight conclusion.

16 **Acknowledgments**

17 [REDACTED]

18 A big thank you to my family, fiancée and friends who have supported me through-
19 out my education. A warm thank you to my friend Joakim Skoog who altered
20 some of the images for me.

21 [REDACTED]

22 [REDACTED]

23 *Linköping, June 2014*
24 *Sven-Patrik Hallsjö*

Contents

Notation

1 Introduction

1.1	Research goals	2
1.2	Theoretical Background	3
1.2.1	Quantum mechanics and quantum field theory	3
1.2.2	Nuclear, particle and subatomic particle physics	4
1.2.3	The standard model of particle physics	4
1.2.4	Dark matter	5
1.2.5	Effective field theory	6
1.2.6	Search for WIMPS	8
1.3	Experimental overview	10
1.3.1	LHC	10
1.3.2	ATLAS	11
1.3.3	Coordinate system	12
1.3.4	Reconstructing data	12
1.3.5	Pile-up	13
1.3.6	Mono-jet analysis	13
1.3.7	Phase II high luminosity upgrade	14
1.3.8	Monte Carlo simulation	15

2 Validation of smearing functions

2.1	Smearing functions	18
2.1.1	Electron and photon	18
2.1.2	Muon	18
2.1.3	Tau	18
2.1.4	Jets	18
2.1.5	Missing Transversal Energy	18
2.2	Validation	20
2.3	Results	21
2.3.1	Electron and photon	22
2.3.2	Muon	23
2.3.3	Tau	23

58	2.3.4 Jets	24
59	2.3.5 Missing Transversal Energy	25
60	2.4 Expected results	26
61	2.5 Discussion	28
62	2.5.1 Smearing independent on pile-up	28
63	2.5.2 Comparison to expected results	28
64	2.6 Conclusion	29
65	3 Evaluating dark matter signals	31
66	3.1 Signal to background ratio	32
67	3.1.1 Selection criteria	32
68	3.1.2 Verifying background data	32
69	3.1.3 Weight	33
70	3.1.4 Figure of merit	33
71	3.1.5 D5 operators	34
72	3.1.6 Light vector mediator models	34
73	3.2 Other selection criteria	35
74	3.2.1 Criteria	35
75	3.2.2 Verifying background data	35
76	3.3 Mitigating the effect of the high luminosity	35
77	3.4 Results	36
78	3.4.1 Verifying background data	36
79	3.4.2 Events	36
80	3.4.3 Limit on M^*	38
81	3.4.4 Effect of pile-up on M^*	39
82	3.4.5 Previous results	40
83	3.4.6 Limit on mediator mass	40
84	3.4.7 Effect of pile-up on mediator mass	41
85	3.5 Discussion	42
86	3.5.1 Comparison to previous results	42
87	3.5.2 Effect of the high luminosity	42
88	3.6 Conclusion	43
89	3.6.1 Limit on M^*	43
90	3.6.2 Limit on mediator mass	43
91	4 Results and Conclusions	45
92	4.1 Validation of smearing functions	45
93	4.2 Signal to background ratio	46
94	4.2.1 Limit on M^*	46
95	4.2.2 Limit on mediator mass	46
96	4.3 Other selection criteria and observables	46
97	4.3.1 Limit on M^*	46
98	4.3.2 Limit on mediator mass	46
99	4.4 Mitigating the effect of the high luminosity	46
100	4.5 Recommendations to mitigate the effect of the high luminosity	46
101	4.6 Suggestions for future research	46

102	A Datasets	49
103	A.1 Background processes	49
104	A.1.1 Validation	49
105	A.1.2 Background to signals	49
106	A.2 Signals	50
107	A.2.1 Qcut	50
108	A.2.2 D5 signal processes	50
109	A.2.3 Light vector mediator processes	50
110	Bibliography	55

Notation

NOTATIONS

Notation	Explanation
barn(b)	1 barn(b)= 10^{-24} cm ²
\oplus	$a \oplus b = \sqrt{a^2 + b^2}$, $a \oplus b \oplus c = \sqrt{a^2 + b^2 + c^2}$

ABBREVIATIONS

Abbreviation	Expansion
ATLAS	A large Toroidal LHC ApparatuS
CERN	Organisation européenne pour la recherche nucléaire ¹
CMS	Compact Muon Solenoid
CR	Control Region
LHC	Large Hadron Collider
MC	Monte Carlo
RMS	Root Mean Square
SM	the Standard Model of particle physics
SR	Signal Region
WIMP	Weakly Interacting Massive Particle
WIMPS	Weakly Interacting Massive ParticleS
QED	Quantum ElectroDynamics
QFT	Quantum Field Theory
QM	Quantum Mechanics

¹Originally, Conseil Européen pour la Recherche Nucléaire

1

Introduction

117 Discrepancies in measurements of the rotations of galaxies indicate the presence
118 of a large amount of matter which interacts through gravity, though not elec-
119 tromagnetically making it invisible to our telescopes. This matter is commonly
120 referred to as dark matter. Since no known or hypothesised particle in the stan-
121 dard model of particle physics can be used as a candidate for dark matter, this
122 hints at the presence of new physics.

123 At the Organisation Européene pour la Recherche Nucléaire (CERN) focus now
124 lies to discover any evidence of so called weakly interacting massive particles
125 (WIMPS) which may be a candidate for dark matter. It is usually impossible to
126 detect any interaction of dark matter candidates on the subatomic scale, however
127 through looking at proposed interactions, searching for assumed decay channels
128 and by investigating what is invisible to the detectors by using momentum con-
129 servation it is hoped that signs will be found. Though to date, none have been
130 found.

131 Both experiments and current theories now show that higher energies are re-
132 quired at the LHC to be able to see any signs. This is why the LHC and all detectors
133 are undergoing a vast upgrade program [1]. In this thesis focus will be on the last
134 part of the upgrade due for completion in 2023, known as the high luminosity-
135 LHC phase II upgrade; and also on the ATLAS detector. The method used in this
136 thesis focuses on looking at data which emulate conditions at the upgraded LHC.

137 1.1 Research goals

138 This research took place at Stockholm University from January 7th until **when**?
139 During the research period the following tasks were set up and performed/answered:

- 140 • Implement a C++ programme that loops over the collisions inside the signal
141 and background datasets.
- 142 • For each collision retrieve the relevant observables (variables used to extract
143 the signal over the background) and apply "smearing functions" to emulate
144 the effect of the high luminosity on the observables.
- 145 • For both signal and background datasets, compare observables before and
146 after smearing. What observables are the least/most affected?
- 147 • Implement selection criteria that selects the signal collisions efficiently while
148 reduces significantly the background. In a first step the selection criteria
149 should be taken from existing studies.
- 150 • Selection criteria can be evaluated and compared with each other using a
151 figure of merit P , that measures the sensitivity of the experiment to the dark
152 matter signal. Calculate P for the given selection criteria before and after
153 smearing.
- 154 • What is the effect of the high luminosity (smearing) on the value of P ?
- 155 • Investigate other selection criteria and observables, to mitigate the effect of
156 high luminosity. Use P to rank different criteria after smearing.
- 157 • Conclude on the effect of the high luminosity on the sensitivity for dark matter
158 and possible ways to mitigate its effects using alternative observables
159 and selection criteria.

1.2 Theoretical Background

1.2.1 Quantum mechanics and quantum field theory

In the beginning of the 20th century, some physical phenomena could not be explained by classical physics, for example the ultra-violet disaster of any classical model of black-body radiation, and the photoelectric effect [2]. It was these phenomena that led to the formulation of quantum mechanics (QM), where energy transfer is quantized and particles can act as both waves and particles at the same time [3].

Combining QM with classical electromagnetism proved harder than expected, colliding a photon(em-field) and an electron (particle/wave) is quite tricky. This can be seen when trying to calculate the scattering between them both in a QM schema. One idea that came from this was to explain them both in the same framework, field theory. Also, trying to incorporate special relativity into QM suggested a field description where space-time is described using the metric formalism from differential geometry. The culmination of both of these problems is the first part of a Quantum field theory (QFT), Quantum electrodynamics (QED) which with incredible precision explains electromagnetic phenomena including effects from special relativity[4]. It is in this merging that antimatter was theorised, since it is a requirement for the theory to hold. After the discovery of antimatter, the theory was set in stone. Since this the theory has been altered somewhat to explain more and more experimental data. This is discussed more in subsection 1.2.2 and subsection 1.2.3.

To be able to calculate properties in QFT one uses the Lagrangian formalism [5], which gives a governing equation for the different physical processes. In general the Lagrangian used for the Standard model is quite complicated, one can thus focus on one of the different terms corresponding to a specific interaction. This can be done to calculate the so called cross-section for a process, which is related to the probability that that process will occur. A step to simplify the calculations is to use the so called Feynman diagrams, an example of which is given in figure 1.1.

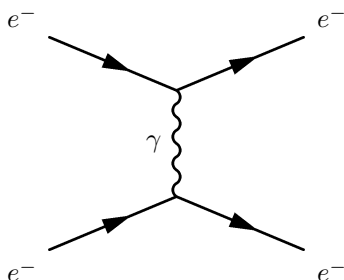


Figure 1.1: An example of a Feynman diagram explaining an electron-electron scattering using QED.

Through the figure, which comes with certain rules, and knowing what the major process (in this case QED) one can calculate the cross-section [4]. It is this that is needed to predict what one will be able to detect new particles.

1.2.2 Nuclear, particle and subatomic particle physics

Many could argue that these branches of physics started after Ernest Rutherford famous gold foil experiment [6], where he discovered that matter is composed of matter with a nucleus, a lot of empty space and electrons.

It was this that sparked the curiosity to see what the nucleus is made of and what forces govern the insides of atoms. After this, and the combination of the theoretical description given by QM, a lot more has been discovered and still more has been predicted. The newest of these is of course the Higgs particle, which was predicted through QFT and then discovered by the ATLAS and the CMS experiments at CERN [7].

The discovered particles are often divided into different groups depending on the fundamental particles that build them up. For instance, particles build up of three quarks are known as hadrons. Particles with an integer spin are known as bosons whereas half-integer particles are known as fermions.

1.2.3 The standard model of particle physics

The standard model of particle physics, referred to simply as the standard model (SM), is the particle zoo which tries to categorize all the particles and that have been discovered experimentally. QFT explains the interactions between these particles and it has also predicted several particles by including symmetries [6]. Regarding SM, Gauge bosons are the force carriers for the different forces, quarks are the and leptons are the fundamental blocks that we know of so far. The difference between the later two is if they interact via the strong force or not.

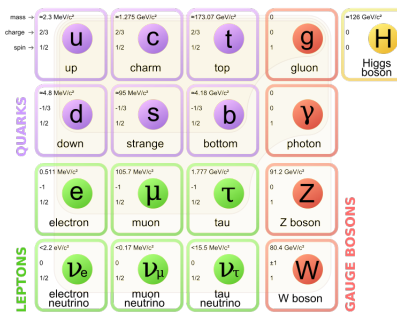


Figure 1.2: The standard model of particle physics where the three first columns represent the so called generations, starting with the first. [8].

SM is today the pinnacle of particle physics and can be used to explain almost everything that occurs around us. There are however some problems [9]:

- There is no link between gravity and the SM.
- Asymmetry between matter and antimatter can not be fully explained.
- No dark matter candidate!
- No explanation that can contain dark matter.

221 In this thesis focus lies with dark matter, some more introduction to possible
 222 dark matter and different candidates in extensions to SM are explained in subsection
 223 1.2.4.

224 1.2.4 Dark matter

225 Dark matter is among other things, the name given to the solution to the discrepancies
 226 of galactic rotations.

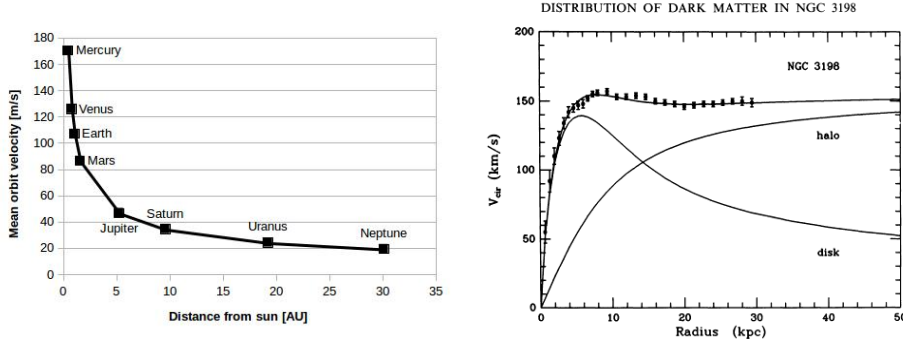
227 To explain this, focus on matter in a galaxy which are rotating around the center
 228 of the galaxy. Through Newtons law of gravity and the centrifugal force one can
 229 calculate the rotation speed dependent on the distance to the center of the galaxy.
 230 Since one of these forces is attractive and the other repulsive, if the matter is in
 231 a stable orbit around the galactic center (which they are) they must be equal and
 232 give us an expression for the speed depending on the distance. Newtons law can
 233 be written as the following:

$$F_{Gravitational} = G \frac{Mm}{r^2} = G_M \frac{m}{r^2} \quad F_{Centrifugal} = m \frac{V^2}{r} \quad (1.1)$$

234 where G is the gravitational constant, M the mass of the centre object, m the mass
 235 of the matter, r the distance between the two and V is the rotation speed. It has
 236 been simplified using G_M since all matter orbits the same galactic center. Setting
 237 the equations in (1.1) results in:

$$G_M \frac{m}{r^2} = m \frac{V^2}{r} \Leftrightarrow V^2 = \frac{G_M}{r} \Rightarrow V = \sqrt{\frac{G_M}{r}} \propto \frac{1}{\sqrt{r}} \quad (1.2)$$

238 where the speed is assumed to be positive and \propto means proportional. Through
 239 these simple calculations it shown that the rotation speed should decrease with
 240 and increased distance. The same reasoning can be applied to our solar system
 241 where this is the case figure 1.3a. The relation in these units is $V = \frac{107}{\sqrt{r}}$ where
 242 107 can be used in (1.2) to calculate the mass of the sun. However when looking
 243 at galaxies, even when taking into account that one has to see the galaxies as a
 244 mass distribution and that the above is only true when outside of the inner mass
 245 half, this is not the case! In figure 1.3b experimental data can be seen from the
 246 galaxy NGC3198 with a fitted curve which does not decrease with the distance
 247 but is instead constant. This is the discrepancy which is solved by postulating
 248 the existence of dark matter. After this the big question arises, what could this
 249 dark matter consist of? What is known so far lies in the name. It is called dark
 250 since there is no electromagnetic interaction and matter since it has gravitational
 251 interaction. This means that it can not be made up of any baryonic matter or
 252 anything in the Standard Model apart from neutrinos. The main interest of this
 253 thesis and also the main contributor to the rotational discrepancies is known as
 254 cold dark matter. This is due to the matter having a low speed, thus low kinetic
 255 energy, and have a high particle mass (In the GeV scale) [9, 12, 13]. This means
 256 however that neutrinos can not be a candidate, thus dark matter can not be made
 257 out of any standard model particles. There are several ideas to detected dark
 258 matter, [9]



(a) *Rotation speed of planets in our solar system. Since the distance is quite small on an astronomical scale, there is no sign of dark matter. Based on data from [10].*

(b) *Rotation speed of matter in NGC3198 with a curve fitting and three different models, if only a dark model halo existed, if there was no dark matter and the correct, if both exist [11].*

Figure 1.3: Different rotation curves, both for planets in our solar system and matter in the NGC3198 galaxy.

- Ordinary matter interacting with ordinary matter can produce dark matter, known as production. Which is the processes that occurs at particle accelerators.
- Dark matter interacting with ordinary matter can produce dark matter, known as direct detection.
- Dark matter interacting with dark matter can produce ordinary matter, known as indirect detection.

In this thesis the focus lies with production. There are several theories how to detect dark matter in proton-proton collisions such that occur at the LHC at CERN this is covered more in subsection 1.2.6.

1.2.5 Effective field theory

In quantum field theory the objective is usually to find the part of the Lagrangian which explains a type of interaction, known as the operator of the interaction and also to find the probability amplitude (cross-section) for a certain interaction. For complicated processes it is easier to employ certain conditions so that the small scale phenomena are simplified and the whole picture understood. This is known as using an effective field theory and the concept is explained in figure 1.4. The operator can be found through assuming the possible interactions and using the effective field theory [4]. The cross-sections can be found through the Feynman diagrams as described in subsection 1.2.1.

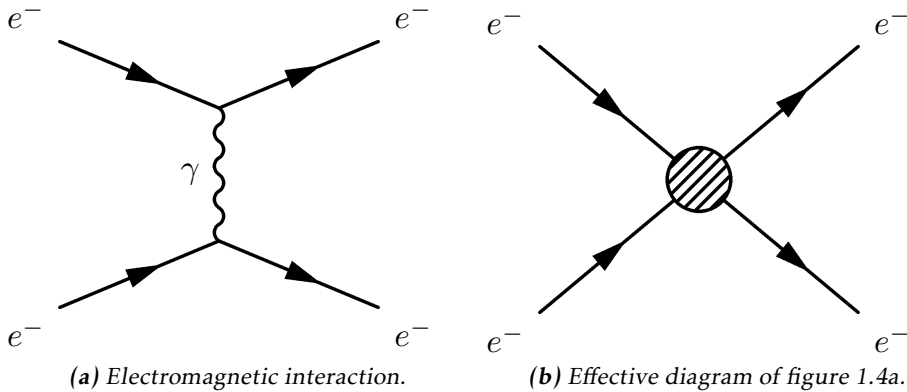


Figure 1.4: Feynman diagram of an electron-electron scattering, both as an ordinary diagram and as its effective theory version, where the details are hidden in the blob.

In this thesis the same effective field theory as in Refs. [12, 14] will be considered. The WIMP (usually denoted χ) is assumed to be the only particle in addition to the standard model fields. It is assumed that an even number of χ must be in every coupling. It is assumed that the mediator exists is heavier than the WIMPS, meaning that their interactions are in higher order terms of the effective field theory and thus not included in the operators. For simplicity, the WIMPS are assumed to be SM singlets, thus invariant under SM gauge transformations, and the coupling to the Higgs boson is neglected.

The operators used in this thesis are assumed to be quark bilinear operators on the form $\bar{q}\Gamma q$ where Γ is a 4×4 matrix of the complete set,

$$\Gamma = \{1, \gamma^5, \gamma^\mu, \gamma^\mu \gamma^5, \sigma^{\mu\nu}\} \quad (1.3)$$

This will dictate how the operators are written, more of why this is done can be found in [4, 12, 14].

This defines an effective field theory of the interaction of singlet WIMPs with hadronic matter. It is an approximation which will break down when the mediator mass is close to the mass of the WIMP. The condition for this is derived in [14] and gives:

$$M > 2m_\chi \quad (1.4)$$

where m_χ is the mass of the WIMP and M is the mass of the mediator particle. There is also the requirement that:

$$M \lesssim 4\pi M_* \quad (1.5)$$

where M_* is the energy scale where the effective theory is no longer a good approximation.

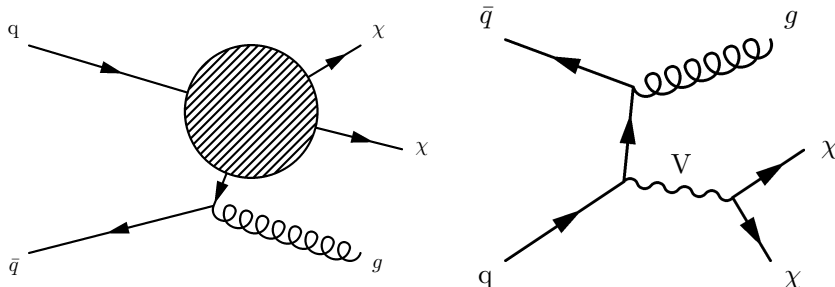
²⁹⁹ In this work, WIMPS are assumed to be Dirac fermions (half integer spin and is
³⁰⁰ not its own antiparticle).

³⁰¹ In table 1.1 the operators which are integrated out via the effective field theory
³⁰² and are of interest in this thesis are given.

Name	Initial state	Type	Operator
D1	qq	scalar	$\frac{m_q}{M_*^3} \bar{\chi} \chi \bar{q} q$
D5	qq	vector	$\frac{1}{M_*^2} \bar{\chi} \gamma^\mu \chi \bar{q} \gamma_\mu q$
D8	qq	axial-vector	$\frac{1}{M_*^2} \bar{\chi} \gamma^\mu \gamma^5 \chi \bar{q} \gamma_\mu \gamma^5 q$
D9	qq	tensor	$\frac{1}{M_*^2} \bar{\chi} \sigma^{\mu\nu} \chi \bar{q} \sigma_{\mu\nu} q$
D11	gg	scalar	$\frac{1}{4M_*^3} \bar{\chi} \chi \alpha_s (G_{\mu\nu}^a)^2$

Table 1.1: Table based on discussion in [13].

³⁰³ Where D denotes that the WIMPS are assumed to be Dirac fermions. These can all
³⁰⁴ be described using figure 1.5a.



(a) Effective Feynman diagram explaining the D-operators. **(b)** Feynman diagram describing the vector mediator model.

Figure 1.5: Feynman diagrams describing the signal models used in this thesis.

³⁰⁵ Another model which is considered is a vector mediator model which is described
³⁰⁶ by figure 1.5b.

1.2.6 Search for WIMPS

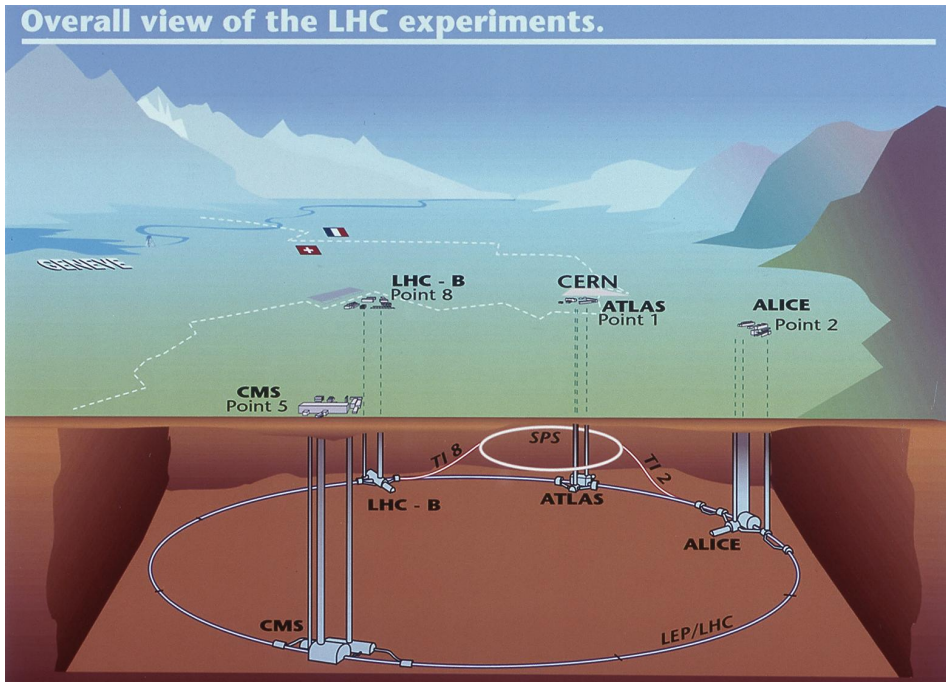
³⁰⁸ The search for WIMPS is based on a mono-jet analysis which is described in sub-
³⁰⁹ section 1.3.6. This method revolves around a high energetic jet which arises from
³¹⁰ the gluon from figure 1.5b and momentum missing from the energy conservation.

- 311 This means that something has happened which the detectors can not detect. If
312 the models from subsection 1.2.5 can explain the missing energy, then a model
313 for WIMPS has been found.
- 314 Since the search for WIMPS at the LHC is based on looking at the missing energy,
315 not actual detection, the experiment can not establish if a WIMP is stable on a
316 cosmological time scale and thus if it is a dark matter candidate [13]. This means
317 that if a candidate is found, it may still not be the dark matter that is needed to
318 explain the cosmological observations.
- 319 The different theories discussed in subsection 1.2.5 require some process in which
320 quarks and anti-quarks are produced. At ATLAS they have looked at proton-
321 proton collisions, in which they are produced, with 8 TeV center of mass energy
322 with out finding any excess of mono-jet events. This is why it is very interesting
323 that the LHC is undergoing a upgrade that will allow higher energy levels, see
324 subsection 1.3.7. With this the processes can be given higher energy and thus the
325 produced particles can be comprised of higher mass.

326 1.3 Experimental overview

327 1.3.1 LHC

328 The large hadron collider (LHC) is a particle accelerator located at CERN near
 329 Geneva in Switzerland, see figure 1.6. The accelerator was built to explore physics
 330 beyond the standard model and to make more accurate measurements of stan-
 331 dard model physics. Before it was shut down for an upgrade in 2012 it was able
 332 to accelerate two proton beams to such a velocity that each proton in them had
 333 an energy of 4 TeV which gives a center of mass energy, $\sqrt{s} = 8$ TeV. The proton
 334 beam is comprised of bunches of protons with enough spacing that bunch col-
 335 lisions can happen independent of each other. Apart from the energy, the rate at
 336 which the accelerator produces a certain process can be calculated through the
 337 instantaneous luminosity. For the LHC the instantaneous luminosity was 10^{34}
 338 $\text{cm}^{-2}\text{s}^{-1}$ [15] or $10\text{nb}^{-1}\text{s}^{-1}$ where 1 barn(b)= 10^{-24} cm^2 .



339 **Figure 1.6:** Figure showing the LHC and the different detector sites[16].

340 The instantaneous luminosity, often just denoted luminosity, can be defined in
 341 different ways depending on how the collision takes place. For two collinear
 intersecting particle beams it is defined as:

$$342 \mathcal{L} = \frac{f k N_1 N_2}{4\pi \sigma_x \sigma_y} \quad (1.6)$$

342 where N_i are the number of protons in each of the bunches, f is the frequency
 343 at which the bunches collide , k the number of colliding bunches in each beam,
 344 and σ_x (σ_y) is the horizontal (vertical) beam size at the interaction point. Since
 345 the instantaneous luminosity increases quadratically with more protons in each
 346 bunch, increasing the number of protons would be a good strategy to increase
 347 the instantaneous luminosity. However aside from the difficulties to create and
 348 maintain a beam with more particles, a large N_i increases the probability for
 349 multiple collisions per bunch crossing, referred to as pile-up. Pile up will be a
 350 key aspect which is described more in subsection 1.3.5.

351 The expected number of events can be calculated by using the instantaneous lu-
 352 minosity through the following:

$$N = \sigma \int \mathcal{L} dt \equiv \sigma \mathcal{L} \quad (1.7)$$

353 where \mathcal{L} is the integrated luminosity and σ is the cross section which is often
 354 measured in barn. The integrated luminosity is a measurement of total number
 355 of interactions that have occurred over time. Before the LHC was shut down \mathcal{L}
 356 was 20.8 fb^{-1} .

357 The cross section, as explained in subsection 1.2.1, is a measure of the effective
 358 surface area seen by the impinging particles, and as such is expressed in units
 359 of area. The cross section is proportional to the probability that an interaction
 360 will occur. It also provides a measure of the strength of the interaction between
 361 the scattered particle and the scattering center. Further details can be found in
 362 reference [17].

363 1.3.2 ATLAS

364 As seen in figure 1.6, there are several detectors at the LHC. One of these is
 365 ATLAS which is a general purpose detector that uses a toroid magnet. Its goal
 366 is to observe several different production and decay channels. The detector is
 367 composed of three concentric sub-detectors, the Inner detector, the Calorimeters
 368 and the Muon spectrometer [18].

369 The Inner detectors main task is to detect the tracks of the particles. It also mea-
 370 sures the position of the initial proton-proton collision.

371 The Calorimeters, electromagnetic and hadronic, are used to calculate the energy
 372 contained in the different particles. The electromagnetic detects particles which
 373 are charged, and the hadronic those which are neutral.

374 The Muon spectrometer is used to detect signs of muons, which will simply pass
 375 through the other detectors without leaving a trace. It also calculates the energy
 376 and momentum of the muons.

377 The neutrinos escape the ATLAS experiment without being detected, and in this
 378 thesis it is assumed that WIMPS pass through all the detectors without leaving
 379 any trace.

380 1.3.3 Coordinate system

381 The coordinate system of ATLAS, seen in figure 1.7 is a right-handed coordinate
 382 system with the x-axis pointing towards the centre of the LHC ring, and the z-axis
 383 along the tunnel/beam (counter clockwise) seen from above. The y-axis points up-
 384 ward. The origin is defined as the geometric center of the detector. A cylindrical
 385 coordinate system is also used for the transversal plane, (R, ϕ, Z) . For simplicity
 386 the pseudorapidity of particles from the primary vertex is defined as:

$$\eta = -\ln(\tan \frac{\theta}{2}) \quad (1.8)$$

387 where θ is the polar angle (xz-plane) of the particle direction measured from
 388 the positive z-axis. η is through this definition invariant under boosts in the z-
 389 direction.

390 It is quite common to calculate the distance between particles and jets in the
 391 (η, ϕ) space, $d = \sqrt{(\Delta\eta)^2 - (\Delta\phi)^2}$.

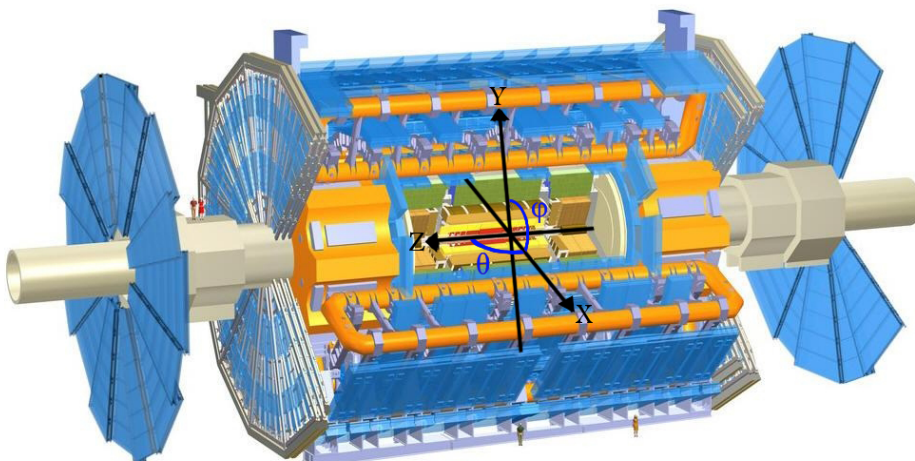


Figure 1.7: The ATLAS detector and the definition of the orthogonal Cartesian coordinate system. Image altered from[19]

392 1.3.4 Reconstructing data

393 To be able to compare the simulated data to real data it is important to include
 394 effects of the detectors. This is done using so called smearing functions which try
 395 to emulate the reconstruction of data.

396 The reconstruction process of data [18] is based on what response is given from
 397 the detectors. It is affected by pile-up and the energy of that which is detected.
 398 This process is not specifically used in the thesis, however the smearing functions
 399 are discussed in section 2.1.

400 1.3.5 Pile-up

401 Pile-up is the phenomena that several proton-proton collisions occur simultaneously.
 402 The number of pile-up is defined as the average number of proton-proton
 403 collisions that occur per bunch crossing per second. It is denoted as $\langle \mu \rangle$. μ can
 404 be calculated by adjusting a Poisson distribution to fit the curve created by the
 405 number of interactions per bunch crossing at a given luminosity. When this is
 406 done μ will be the mean value of the Poisson distribution.

407 1.3.6 Mono-jet analysis

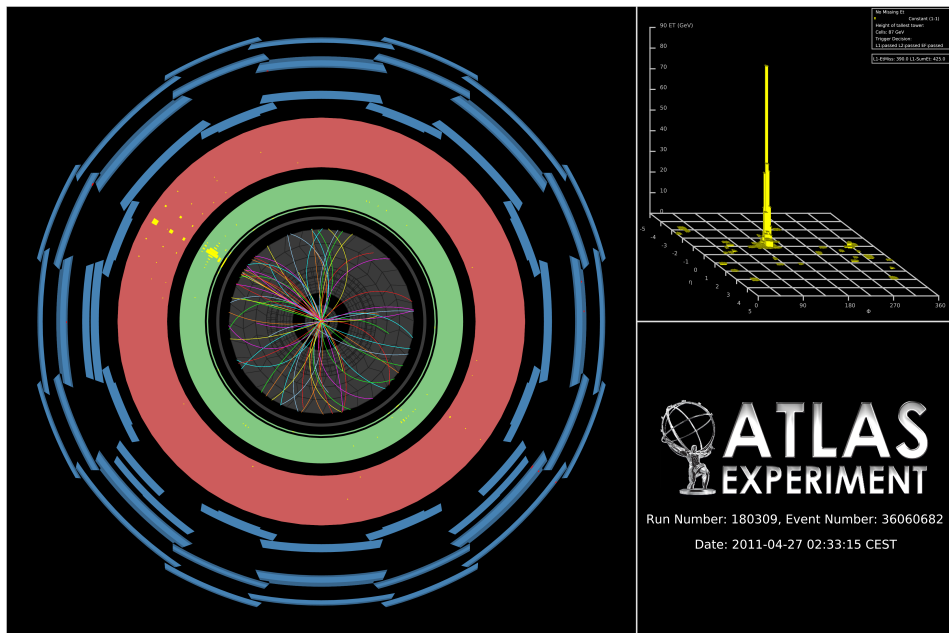


Figure 1.8: Image of an actual mono-jet event recorded by the ATLAS experiment [20].

408 When measuring the transversal energy one can in some interactions find incon-
 409 sistencies, such as jets that are in excess in one direction. In figure 1.8 one can see
 410 a high energetic jet which gives an excess of transversal energy in one direction
 411 after the collision. Since there is no balancing jet there must be transverse energy
 412 that is not detected, denoted E_T^{Miss} , since it was close to zero before the collision.
 413 This gives an indication that there energy to balance this that simply can not be
 414 detected. This could for instance be neutrinos or the sign of a new particle.

415 E_T^{Miss} is the modulus of the E_T^{Miss} vector which is defined as:

$$E_T^{\vec{M}iss} = -\sum E_T^{\vec{jet}} - \sum E_T^{\vec{Electron}} - \sum E_T^{\vec{\mu}on} - \sum E_T^{\vec{T}au} - \sum E_T^{\vec{\gamma}on} \quad (1.9)$$

416 Jets are hadrons which travel in the same direction and are usually created from

hadronization of a quark or a gluon in a collision. Usually jets are composed of a lot of energetic hadrons.

Since the jets are created from quarks or gluons, measuring a jet results in more information about the collision.

There are two main classes of events, signal and background. The signal corresponds to events that would arise from one of the processes in subsection 1.2.5. However to know that the missing energy is sign of the signal then one must understand all the other components that could contribute to the missing energy. Also there must be an excess of missing energy from what is expected from the background.

The background comprises of standard model processes that can mimic the mono-jet signature.

1.3.7 Phase II high luminosity upgrade

At the moment, the whole LHC is undergoing a step by step upgrade program which will be finalized around 2022-2023, denoted the high luminosity upgrade, or HL-upgrade. The upgrade consists of different stages, meaning that the upgrade will halt for periods so that experiments can take place. In figure 1.9 one can see

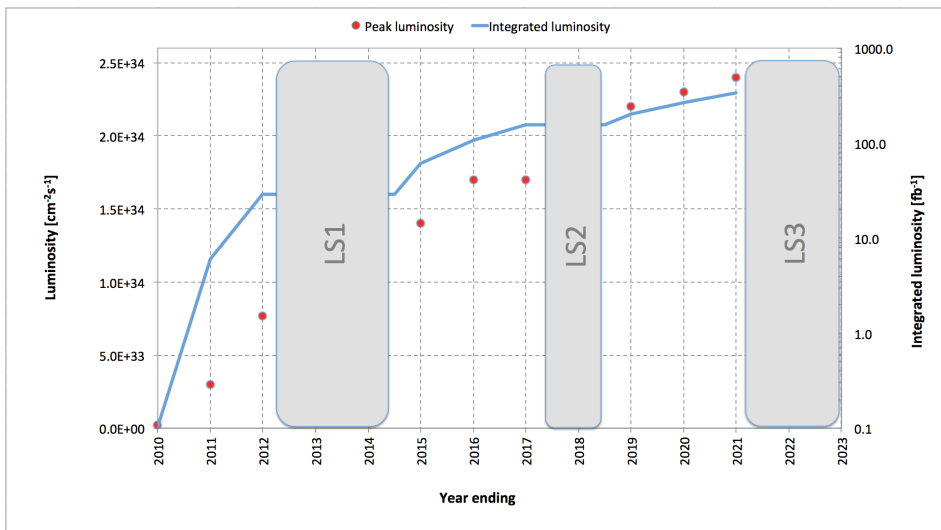


Figure 1.9: A graph showing the upgrading timetable with the instantaneous luminosity, denoted luminosity, and integrated luminosity expected in the different stages.

the three proposed upgrades. The period before LS1 is denoted phase 0, after LS1 and before LS2 phase I and after LS3 phase II.

LS1 is the upgrade which will take the LHC to its designed performance.

- 437 LS2 will take the LHC to the ultimate designed instantaneous luminosity.
 438 LS3 which is the focus of this thesis, will increase the instantaneous luminosity
 439 even more. Though for this to happen a modification of the whole LHC
 440 must be done, instead of just an upgrade and maintenance as before.

441 The following is expected for the experiments done after phase II:

Entity	Expected	Last run (2012)
Instantaneous luminosity	$\mathcal{L} \sim 50 \text{ nb}^{-1} \text{s}^{-1}$	$\mathcal{L} \sim 10 \text{ nb}^{-1} \text{s}^{-1}$
Integrated luminosity	$\mathcal{L} = 1000 - 3000 \text{ fb}^{-1}$	$\mathcal{L} = 20 \text{ fb}^{-1}$
Pile-up	$\langle \mu \rangle = 140$	$\langle \mu \rangle = 20$
Center of mass energy	$\sqrt{s} = 14 \text{ TeV}$	$\sqrt{s} = 8 \text{ TeV}$

Table 1.2: Expected running values for the Phase II HL-upgraded LHC with older values for comparison [21].

442 Where it should be noted that the integrated luminosity indicates the total amount
 443 of data which will be collected after the upgrade is completed before the next up-
 444 grade takes place.

445 1.3.8 Monte Carlo simulation

- 446 As mentioned before, in this thesis only emulated data has been used. This data
 447 is created by using a Monte Carlo (MC) simulation of the background processes
 448 and the expected signal. To do this a program called MadGraph is used.
 449 MadGraph [22] starts with Feynman diagrams and then generates simulated events
 450 based on lots of different parameters.
 451 PYTHIA [23] is a package which adds the correct description of jets to MadGraph
 452 by including hadronization. The correct description of pile-up comes from other
 453 ATLAS software.
 454 The tool to access all this data and analyse it a tool called ROOT, which is used
 455 for programming high energy physics related tools [24].

2

Validation of smearing functions

458 A full detector simulation of the ATLAS detector based on the GEANT [25] pro-
459 gram makes it possible to obtain the expected detector responses to electrons,
460 muons, tau leptons, photons (γ) and jets of hadrons. However these simulations
461 are extremely time-consuming and require a lot of computing power. Also at the
462 present time only a limited set of these simulations exists for the ATLAS phase II
463 upgrade.

464 In this thesis a different strategy is used. Instead of performing a full detector
465 simulation the observed particles from the event generator, which simulates the
466 proton-proton collisions, are smeared by using random numbers following reso-
467 lution functions specific to each type of particle. These emulate how the detector
468 and the reconstruction is affected by the increased luminosity and the pile-up
469 which comes with this.

470 The resolution functions or smearing functions are the official functions devel-
471 oped from previous studies [1, 26] by the ATLAS collaboration for the study of
472 the ATLAS phase II upgrade. The key feature of those studies was that the di-
473 rection of the momenta is unaffected and that only jets and E_T^{Miss} are affected by
474 pile-up. Since this was confirmed in previous studies it was not incorporated into
475 the smearing functions as discussed more in section 2.1.

476 Since part of this thesis work was to take the official ATLAS smearing functions
477 and apply the smearing to each particle, it was important to check that the en-
478 ergy and momenta resolutions of the smeared objects were consistent with the
479 expected values. Thus in this chapter the energy and momenta resolutions are
480 measured after applying the smearing to some simulated processes and the re-
481 sulting resolutions are compared with the expected values.

482 2.1 Smearing functions

483 These smearing functions are designed so that they take into account the effi-
484 ciency of the different detectors, limitations as well as their dependence on pile-
485 up. They also take into account how all this varies depending on the measured
486 entries energy or momenta.

487 Terminology:

- 488 • Data before smearing, simulated data, is denoted as data at a truth level or
489 truth data.
- 490 • Data after smearing, which is comparable to what is measured is denoted
491 as reconstructed or reco data as discussed in subsection 1.3.4.

492 2.1.1 Electron and photon

493 The identification of electrons relies on finding an isolated electron track and
494 a pattern in the calorimeter compatible with an electron shower. Pile-up will
495 affect the electrons by decreasing the efficiency to identify an electron because of
496 the increased number of tracks. However for the identified electrons the energy
497 resolution will be close to that without pile-up.

498 The electron and photon have the same smearing since they are both detected in
499 a similar way.

500 2.1.2 Muon

501 The identification of muons relies on isolated tracks in the inner detector being
502 matched with information in the muon system. Since the muon system is the
503 outer most detector seen from the collision point it is unaffected by the false
504 detection effects of pile-up.

505 2.1.3 Tau

506 Tau is detected similarly to electron and photon. In this thesis all tau processes
507 are assumed to be at 3 prong. Where prong refers to the different amount of
508 tracks from which they were reconstructed. This in turn means that the effect of
509 pile-up will be worse compared to an electron as a triplet must be found in an
510 increased number of tracks.

511 2.1.4 Jets

512 The largest effect of pile-up is to add additional jets in the ATLAS detector. These
513 additional jets contribute to additional energy deposited inside the existing jets
514 and to E_T^{Miss} .

515 2.1.5 Missing Transversal Energy

516 E_T^{Miss} , the missing transversal energy, which was discussed in subsection 1.3.6,
517 and defined in (1.9) is calculated by knowing that there should be energy conser-

518 vation in the collision. It is comprised of different parts, one from neutrinos, one
519 from errors in the other measurements and one from new physics. It should be
520 affected by pile-up as described above.

521 2.2 Validation

522 To validate the smearing functions a comparison with Ref. [26] was made where
 523 the standard deviation, depending on the energy or momentum value of an entity,
 524 was given, see section 2.4. This is performed using the simulated processes listed
 in table 2.1.

Table 2.1: Different processes from
 where data has been taken. Each
 sample is a simulation of a physical
 process, the simulation names can
 be found in appendix A

Particle	Process
Electron	$W \rightarrow e\nu$
Muon	$W \rightarrow \mu\nu$
Tau	$W \rightarrow \tau\nu$
γ	$\gamma + \text{Jet sample}$
Jets	Jet sample
E_T^{Miss}	$Z \rightarrow \nu\nu + \text{Jet sample}$

525
 526 The energy and momentum resolutions are obtained for each type of particle by
 527 comparing the values before and after smearing. This is done looking at the reco
 528 data for a given slice at a truth energy or momentum value. Since the smearing
 529 functions takes a lot into account the match will not be a fine line as seen in
 530 figure 2.3b.

531 By fitting a Gaussian curve to this data will then result in the standard deviation
 532 which is used in the validation. The standard deviation is also known as the
 533 resolution of the data and will be denoted σ .

534 This resolution is then compared to previous results, [26].

535 To get enough statistics enough data must be available for a given truth energy
 536 or momenta and the analysis must be specific enough to only look at a narrow
 537 enough interval around this point.

538 2.3 Results

- 539 As discussed above, the method was to plot the data against its smeared counter-
540 part and through this determine σ to see if it conforms to the expected values.
- 541 Only one energy value is shown for simplicity, though the comparison was done
542 for different energy values.
- 543 The average number of pile-up is fixed at 60 as a benchmark unless anything else
544 is stated.
- 545 As the comparison, figure 2.4, figure 2.1, figure 2.2 and figure 2.5 are divided
546 depending on the different η values.
- 547 All results are summarized in table 2.5.

548 2.3.1 Electron and photon

549 Since these interact very similarly in the detector, their smearing functions are
 550 identical. The slice value represents at which value of unsmeared energy or mo-
 551 mentum this smearing occurs.

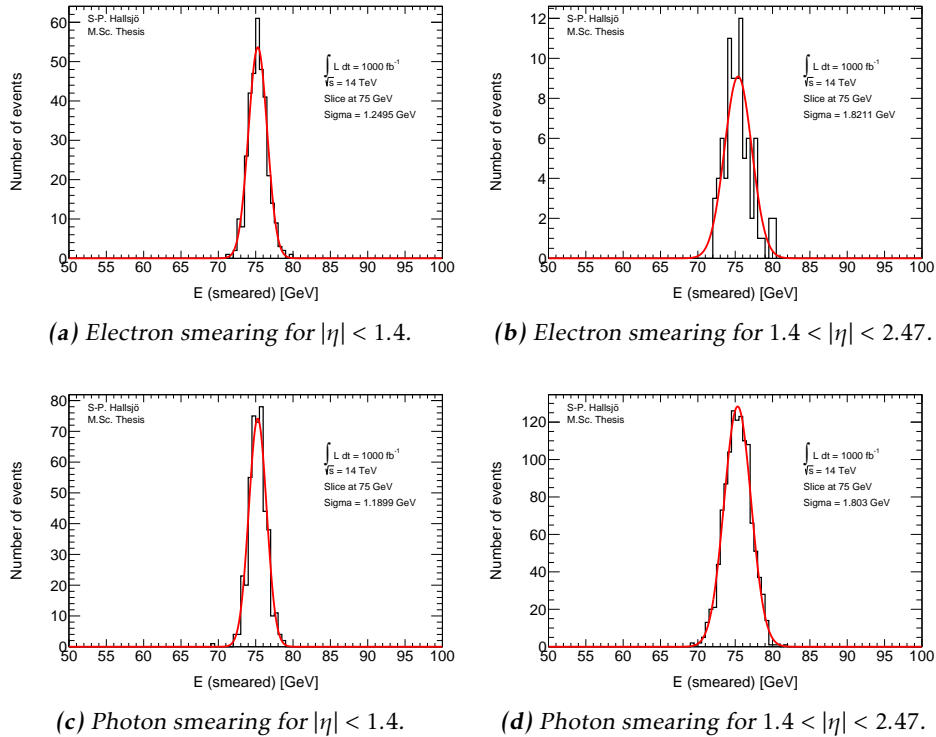


Figure 2.1: Photon and electron smearing plots.

552 **2.3.2 Muon**

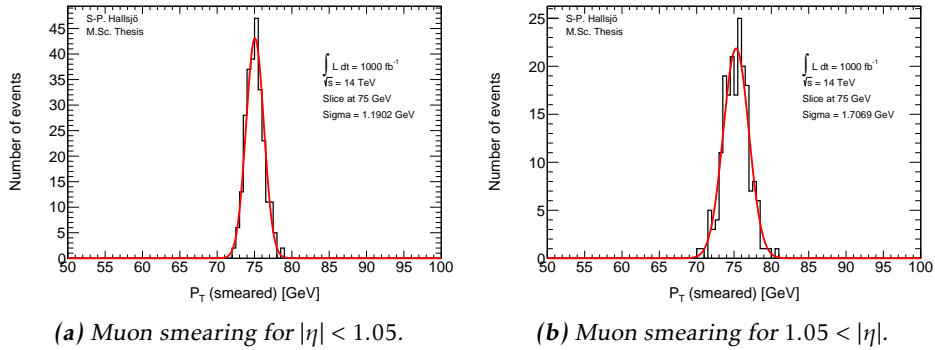


Figure 2.2: Muon smearing plots.

553 **2.3.3 Tau**

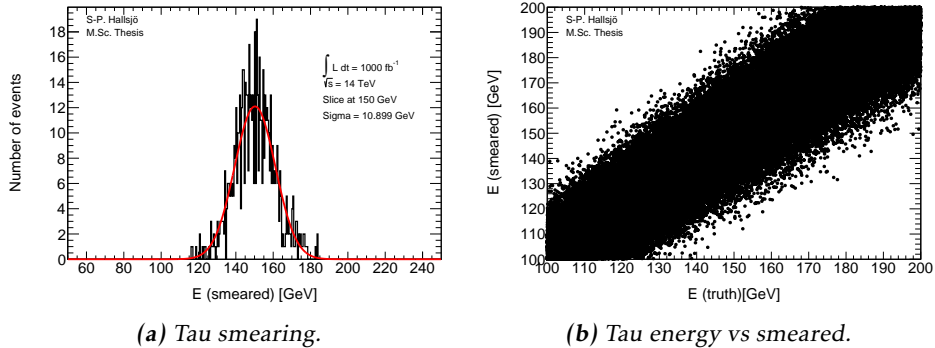


Figure 2.3: Tau smearing and energy vs smearing plot.

2.3.4 Jets

Jets as described in subsection 1.3.6, are hadronic showers. The smearing functions are divided into four different regions depending on the angle η .

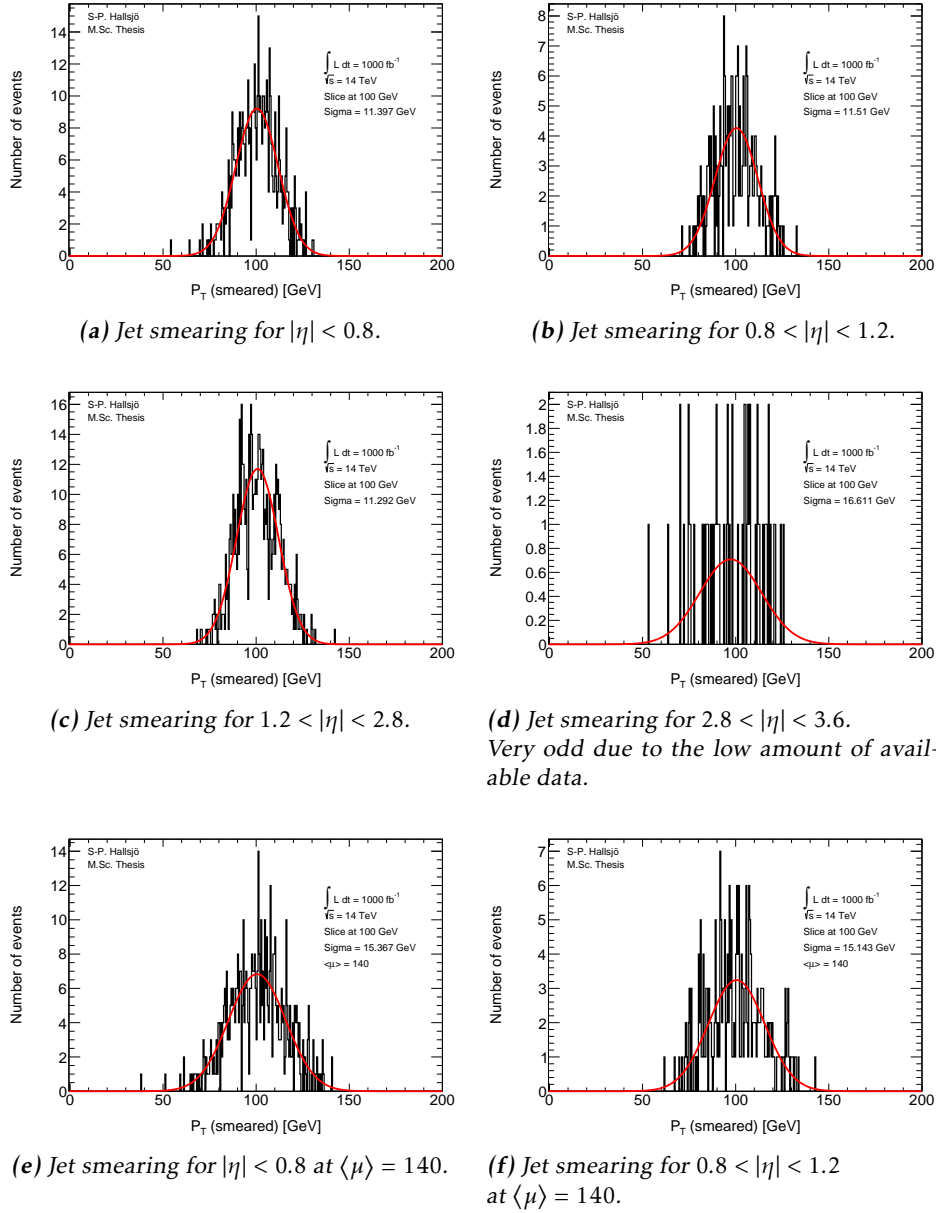


Figure 2.4: Jet smearing plots.

557 2.3.5 Missing Transversal Energy

558 These figures are given as smeared value from origin, thus at 0 it represents that
 559 the energy is unsmeared, compared to the others where the slice value represents
 560 the unsmeared.

561 Here the E_T^{Miss} is projected down to the x- and y-axis, since these are the transver-
 562 sal axes, to be smeared.

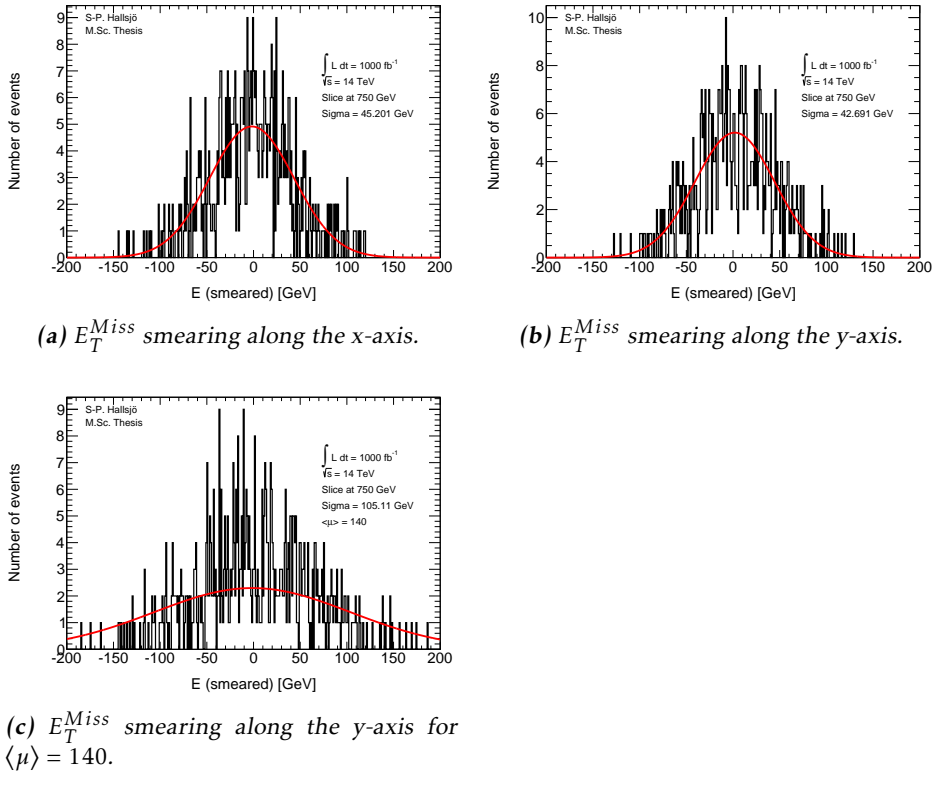


Figure 2.5: E_T^{Miss} smearing plots

2.4 Expected results

563 The expected response has been calculated and taken from [26].

564 The independence of pile-up for leptons and photons is backed up in previous
565 research, for instance [1, 27] were the first states:

566 “The uncertainty due to pile-up was investigated by comparing
567 simulated MC samples with and without pile-up and was found to be
568 negligible”
569

570 To validate the smearing code comparisons were made with [26] which gave the
571 following formulation for the expected σ :

Observable	Absolute σ
Electron & photon	$\sigma = 0.3 \oplus 0.1\sqrt{E(GeV)} \oplus 0.01E(GeV), \eta < 1.4$ $\sigma = 0.3 \oplus 0.15\sqrt{E(GeV)} \oplus 0.015E(GeV), 1.4 < \eta < 2.47$
Muon momentum	$\sigma = \frac{\sigma_{id}\sigma_{ms}}{\sigma_{id} \oplus \sigma_{ms}}$ $\sigma_{id} = P_T(a_1 \oplus a_2 P_T)$ $\sigma_{ms} = P_T(\frac{b_0}{P_T} \oplus b_1 \oplus b_2 P_T)$
Tau energy	$\sigma = (0.03 \oplus \frac{0.76}{\sqrt{E(GeV)}})E(GeV)$, for 3 prong.
Jet momentum	$\sigma = P_T(GeV)(\frac{N}{P_T} \oplus \frac{S}{\sqrt{P_T}} \oplus C)$ where $N = a(\eta) + b(\eta)\mu$
E_T^{Miss}	$\sigma = (0.4 + 0.09\sqrt{\mu})\sqrt{\sum E(GeV) + 20\mu}$

Table 2.2: Expected absolute σ where the parameters are given for muons in table 2.3 and for jets in table 2.4. Functions take from [26].

	a_1	a_2	b_0	b_1	b_2
$ \eta < 1.05$	0.01607	0.000307	0.24	0.02676	0.00012
$ \eta > 1.05$	0.03000	0.000387	0.00	0.03880	0.00016

Table 2.3: Parameters used in the muon smearing function taken from [26].

$ \eta $	a	b	s	C
0-0.8	3.2	0.07	0.74	0.05
0.8-1.2	3.0	0.07	0.81	0.05
1.2-2.8	3.3	0.08	0.54	0.05
2.8-3.6	2.8	0.11	0.83	0.05

Table 2.4: Parameters used in the jet smearing function taken from [26].

Process	σ [GeV]	Expected σ
Electron low η	1.25 ± 0.05	1.18
High η	1.82 ± 0.14	1.74
Photon low η	1.19 ± 0.04	1.18
High η	1.80 ± 0.04	1.74
Muon low η	1.19 ± 0.05	1.50
High η	1.71 ± 0.09	2.18
Tau	10.90 ± 0.31	10.34
Jet low η	11.40 ± 0.35	11.60
$\langle \mu \rangle = 140$	15.37 ± 0.47	15.77
Mid low η	11.51 ± 0.52	11.94
$\langle \mu \rangle = 140$	15.14 ± 0.68	15.95
Mid high η	11.29 ± 0.31	10.94
High η	16.61 ± 1.53	13.50
E_T^{Miss} x-axis	45.20 ± 1.35	48.45
E_T^{Miss} y-axis	42.69 ± 2.28	48.45
$\langle \mu \rangle = 140$	105.11 ± 12.24	87.28

Table 2.5: σ values.

- 572 • Where the given σ is still the absolute.
- 573 • Where the large difference between calculated and expected σ for Muons
574 and E_T^{Miss} is explained by incorrectly calculated errors in σ .

575 2.5 Discussion

576 2.5.1 Smearing independent on pile-up

577 From the validation done it was interesting to note that the smearing functions
578 were created from previous studies, [1, 27], which had shown that leptons and
579 photons are not affected by pile-up. This may seem incredible however it be-
580 comes quite logical when one understands how the detectors work. To be able to
581 detect particles the detectors must detect an excess of energy which comes from
582 a particle passing through. This should not be distorted by an increased pile-up.
583 The amount of particles passing through will of course increase, but the detec-
584 tions should be unaffected as well as the recreation of the events. However with
585 the same logic it makes sense that jets and E_T^{Miss} are quite affected since they
586 are combined of several parts, either hadronic particles or by all the transversal
587 missing energy.

588 Another interesting part is how the effect diminishes with and increasing energy.
589 As seen above, and through the the formula, for the high energies which were of
590 interest here the effect is minimal.

591 2.5.2 Comparison to expected results

592 One of the major problems in the comparison was to get the significance of the
593 Gaussian fit to be calculated correctly. The tool ROOT has a lot of different fea-
594 tures which made this task somewhat difficult. Also since this is a statistical
595 property there is a statistical fluctuation in the result.

596 Another was to retrieve the correct values from the paper, [26], since it was un-
597 clear if the values given were absolute or scale dependent. This has now been
598 corrected in a new version of the paper.

599 **2.6 Conclusion**

600 The smearing functions work as intended within 5.8 sigma, however when using
601 a test box and averaging the sigmas one ends up with half of this for the extreme
602 cases, muons and E_T^{Miss} y-axis.

3

Evaluating dark matter signals

605 **Disclaimer: All data provided is still a work in progress and may be subject to
606 change before the final version.**

607 The main goal of the thesis is to investigate if certain dark matter signals can
608 be detected after the high luminosity upgrade. One immediate worry is that the
609 background will be large in comparison to the signal, making the signal undetectable.
610

611 The signal models are given in appendix A along with the background models.
612 The different models were discussed in part in subsection 1.2.5 and some more
613 in this chapter.

614 This thesis focus on using a luminosity at 1000 fb^{-1} and a center of mass energy
615 at 14 TeV. The reco data is created using a pile-up rate, $\langle \mu \rangle = 140$ as expected
616 during phase II.

617 Each of these has been evaluated in different signal regions and the detectability
618 has been evaluated using a statistical P-value. This process has been performed
619 at different pile-up values.

620 3.1 Signal to background ratio

621 3.1.1 Selection criteria

622 For different purposes different selection criteria or regions are used. These are a
 623 set of criteria specified to enhance the area of interest. For instance, if simulating
 624 a specific signal one wants to find as many ways as possible to diminish the back-
 625 ground. This so that when searching experimentally, the signal will be easier to
 626 detect.

627 These can be quite general cuts, there are only some things to take into consider-
 628 ation.

- 629 • If experimental, what limitations are set by the detectors? Are there some
 630 criteria already?
- 631 • If simulated, is there some criteria set in the generator?
- 632 • Are there criteria which must be set since there is to much uncertainty in
 633 the data? or a large effect of pile up?

634 3.1.2 Verifying background data

635 To verify that the background data was correct it was compared with Ref. [28]
 636 in which the center of mass energy is 8 TeV and the luminosity is 10 fb^{-1} . Since
 637 the luminosity is not 1000^{-1} as used in this thesis the expected values from the
 638 paper scaled up with a factor 100 to be comparable.

639 Somewhat unexpectedly a center of mass energy at 8 TeV required the cross-
 640 sections to be a factor 4 lower than the cross-sections at 14 TeV. **How do I ref-**
641 erence the cross-section?

The signal regions used in the article were the following:

Selection Criteria		
Jet veto, require no more than 2 jets with $p_T > 30 \text{ GeV}$ and $ \eta < 4.5$		
Lepton veto, no electron or muon		
Leading jet with $ \eta < 2.0$ and $\Delta\phi(\text{jet}, E_T^{\text{miss}}) > 0.5$ (second-leading jet)		
signal region	SR3p	SR4p
minimum leading jet p_T (GeV)	350	500
minimum E_T^{miss} (GeV)	350	500

642 **Table 3.1:** The signal regions from Ref. [28].

643 The article had in total four signal regions, unfortunately since the simulated
 644 events used in this thesis are filtered before the analysis only the two highest
 645 regions are comparable. This can be seen in subsection 3.4.1 in table 3.3.

646 **3.1.3 Weight**

647 A weight is used to normalize different types of data so that they can be compared.
 648 In thesis the following is used:

$$649 \text{weight} = \frac{\mathcal{L}\sigma}{N_{Raw}} \quad (3.1)$$

650 where N_{Raw} is number of events expected at the luminosity that was set to create
 651 the data, compared to \mathcal{L} which is the luminosity at which the data is compared
 652 and σ is the cross-section.

652 **3.1.4 Figure of merit**

653 To be able to evaluate different signal regions and different signal models, a figure
 654 of merit p is used. The value p is the probability for an assumed hypothesis
 655 to be correct, thus a good signal region will yield a low value. The assumed
 656 hypothesis is that the background and its fluctuations is measured over the signal
 657 plus background.

658 Assuming the expected number of background events are $B \pm \sigma_B$ where σ_B is the
 659 quadratic sum of the statistical error from Monte Carlo, the statistical error from
 660 the control region (CR) and the systematic errors. The expected number of signals
 661 is S , assumed without fluctuation.

662 If no uncertainty in B or S is assumed, then the number of expected events, N , in
 663 the signal region should follow a Poisson distribution as such:

$$664 P(N|S+B) = \frac{e^{-(S+B)}(S+B)^N}{N!} \quad (3.2)$$

665 However since there is an uncertainty in the background, the probability distribution
 666 $P(N|S+B)$ must be convoluted with a Gaussian function:

$$667 G(N_B|B, \sigma_B) = \frac{1}{\sigma_B \sqrt{2\pi}} e^{-\frac{(N_B-B)^2}{2\sigma_B^2}} \quad (3.3)$$

where N_B is the expected number of background events. The convolution is done
 using N_B as N resulting in the total probability density function:

$$668 F(N|S+B, \sigma_B) = P(N|S+N_B)*G(N_B|B, \sigma_B) = \\ = \int_{-\infty}^{\infty} P(N|N_B - (S+B))G(N_B|B, \sigma_B)dN_B \quad (3.4)$$

669 This leads to the probability of the signal plus background fluctuation to B events
 670 being obtained by summing the probability function from $N=0$ to $N=B$.

$$671 p = \sum_{i=0}^B \int_{-\infty}^{\infty} P(i|N_B - (S+B))G(N_B|B, \sigma_B)dN_B \quad (3.5)$$

In this thesis, two different models of the error in the background σ_B are used. Both models are based on Ref. [28]. As described in the beginning of this subsection the error is calculated as:

$$\sigma_B = \text{Statistical error from MC} \oplus \text{Statistical error in CR} \oplus \text{Systematic error}$$

- The statistical error from MC has been neglected since there is no way of estimating it for the used data.
- The statistical error from background CR has been assumed to decrease with the increased luminosity, $\frac{30}{380} \frac{\sqrt{L_{old}}}{\sqrt{L_{new}}}$
- The systematic error has been given two different values, from the article: $\frac{30}{380}$ or fixed at 0.02.
- All this results the total error being used as either, 0.0793411 or 0.0215018.

3.1.5 D5 operators

As described in the introduction subsection 1.2.5, one of the signals is modelled using the D5 operator. In this thesis two different scenarios were used, one at a dark matter mass of 50 GeV and one at 400 GeV.

Each of these models are modelled with a mass suppression scale, denoted M^* , which is strongly correlated to the cross-section of the process.

One property which is of interest is to calculate how large M^* can be so that the signal is still detectable over the background processes. These results are given in subsection 3.4.3.

3.1.6 Light vector mediator models

As described in the introduction subsection 1.2.5, the other signal model is a vector mediator model. In this thesis these signals have two different width scenarios and a number of different mediator mass scenarios. In addition to this there are, as with the D5 operator two different dark matter mass scenarios.

What is width?

The models which are detectable are given in subsection 3.4.6.

691 3.2 Other selection criteria

692 3.2.1 Criteria

693 To be able to compare signal results to previous papers new signal regions were
 694 devised. It was also discovered that the requirement of no electrons was to harsh
 695 for the signal models. Because of this new signal criteria were devised.

Selection Criteria

Jet veto, require no more than 2 jets with $p_T > 30\text{GeV}$ and $|\eta| < 4.5$

Lepton veto, no electron or muon.

The electron veto is defined: $\Delta R(jet^{lead}, electron^{lead}) \geq 0.4$ and
 $electron^{lead} p_T > 20\text{GeV}$ removed.

Leading jet with $|\eta| < 2.0$ and $\Delta\phi(jet, E_T^{Miss}) > 0.5$ (second-leading jet)

signal region	SR1	SR1p	SR2	SR3	SR4
minimum leading jet p_T (GeV)	350	500	600	800	1000
minimum E_T^{Miss} (GeV)	350	500	600	800	1000
signal region	SRa		SRb	SRc	SRd
minimum leading jet p_T (GeV)	350		350	350	350
minimum E_T^{Miss} (GeV)	350		600	800	1000

Table 3.2: The new signal regions

696 3.2.2 Verifying background data

697 To make sure that the altered electron veto still produces results comparable with
 698 [28] a comparison was made again. This can be seen in subsection 3.4.1 in ta-
 699 ble 3.4.

700 3.3 Mitigating the effect of the high luminosity

701 As discussed in subsection 2.5.1 the effect of pile-up should be minimal in the
 702 high energy regions which are of interest in this thesis.

703 Mention that the effect is on a trigger level, that the lowest SR will be lost.

704 Even though this was envisioned as the primary focus of the thesis, it was shown
 705 that the effect of pile-up is minute for these high signal regions. Thus the focus
 706 was shifted to perform a more in-depth mono-jet analysis of different DM signal
 707 models.

708 3.4 Results

709 3.4.1 Verifying background data

710 In table 3.3 a comparison has been made. It can be seen that the simulated events
 711 and expected events coincide on all accounts apart from $W \rightarrow \tau\nu$, $W \rightarrow \mu\nu$ and
 712 thus the total as well. **This can be explained by better separation of μ, τ and**
 713 **missing energy.** Tau can not be reconstructed as jets in the code, they can in
 714 reality!

715 Here used truth data as to not be effected by pile-up.

Process	SR3p	Expected SR3p	SR4p	Expected SR4p
$Z \rightarrow \nu\nu$	140298	152000	25250.3	27000
$W \rightarrow \tau\nu$	40700.8	37000	5861.74	3900
$W \rightarrow e\nu$	11229	11200	1506.58	1600
$W \rightarrow \mu\nu$	13727.1	15800	1872.32	4200
Total background	205955	218000	34491	36700

Table 3.3: Comparison of the simulated and expected events from [28] with $\mathcal{L} = 1000\text{fb}^{-1}$, cross-sections corresponding to $\sqrt{s} = 8\text{TeV}$ and using the same electron veto.

Process	SR1	Expected SR1	SR1p	Expected SR1p
$Z \rightarrow \nu\nu$	147009	152000	26734	27000
$W \rightarrow \tau\nu$	44727.7	37000	6543.82	3900
$W \rightarrow e\nu$	17964	11200	2470.46	1600
$W \rightarrow \mu\nu$	14285.7	15800	1971.87	4200
Total background	223986	218000	37720.2	36700

Table 3.4: Comparison of the simulated and expected events from [28] with $\mathcal{L} = 1000\text{fb}^{-1}$, cross-sections corresponding to $\sqrt{s} = 8\text{TeV}$ and using a modified electron veto.

716 3.4.2 Events

717 Give a table with the number of events for signals and background in all signal
 718 regions both truth and reco.

719 The below is only for truth, must create new code to write it for reco.

720 Have a table with the number of signal and bkg ground events for the different
 721 SR where the signal then is given at $M^* 1\text{ GeV}$ for a good comparison.

722 Same tables as above but at reco.

Process	SRa/SR1	SRb	SR2	SRc	SR3	SRd	SR4
D5 mDm=50 $Q_{cut} = 200$	50410.4	434.012	0	0	0	0	0
M*=1TeV $Q_{cut} = 400$	53242.1	10018.1	4934.73	159.539	0	22.0054	0
$Q_{cut} = 600$	26210.6	25958.1	25284.7	12767.2	10749.7	5199.47	4391.35
Total signal	129863	36410.1	30219.4	12926.8	10749.7	5221.48	4391.35
Z $\rightarrow \nu\nu$	604479	58613.9	42656.5	11383.4	8423.89	2842.85	2110.55
W $\rightarrow \tau\nu$	154140	10678.5	7807.06	1788.16	1307.89	385.861	295.124
W $\rightarrow e\nu$	61771.6	3961.35	2890.39	653.918	485.485	152.221	109.887
W $\rightarrow \mu\nu$	49114.3	3051.61	2357.17	498.995	379.201	108.086	90.9721
Total background	869505	76305.4	55711.2	14324.5	10596.5	3489.02	2606.54

Table 3.5: Signal and background events for truth data in the signal regions.

Process	SRa/SR1	SRb	SR2	SRc	SR3	SRd	SR4
D5 mDm=50 $Q_{cut} = 200$	41968.9	564.215	0	0	0	0	0
M*=1TeV $Q_{cut} = 400$	52235.9	13131.8	4126.01	275.068	0	22.0054	0
$\langle\mu\rangle = 140$ $Q_{cut} = 600$	26090	25065.8	23893	13477.1	9978.04	5482.88	4130.4
Total signal	120295	38761.9	28019	13752.2	9978.04	5504.88	4130.4
Z $\rightarrow \nu\nu$	553735	71613.2	39104.6	13145.1	7680.99	3139.89	1932.33
W $\rightarrow \tau\nu$	156023	14500.3	7741.1	2174.02	1282.23	467.433	275.877
W $\rightarrow e\nu$	58873.9	5177.33	2705.75	789.925	447.655	175.639	106.284
W $\rightarrow \mu\nu$	47800.6	4030.7	2298.63	617.889	380.102	138.71	89.1707
Total background	816433	95321.6	51850	16727	9790.98	3921.67	2403.66

Table 3.6: Signal and background events for reco data with $\langle\mu\rangle = 140$ in the signal regions.

723 **Disclaimer: The thesis is not completed after here.**

724 **3.4.3 Limit on M^***

725 The mass suppression scale.

726 Give at 1000fb-1 and with 14 TeV cross-sections. And for the different signal
727 regions. Refer to M^* explained in subsection d5. subsection 3.1.5

728 For the new signal regions: **Include a table of the limits for truth and Reco.**

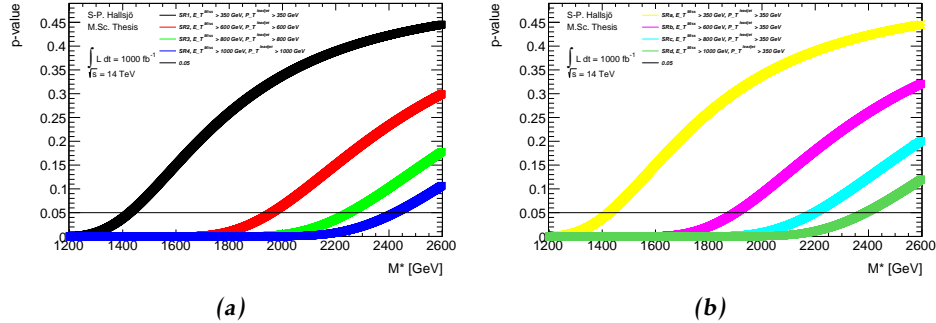


Figure 3.1: On a truth level error model 0.02.

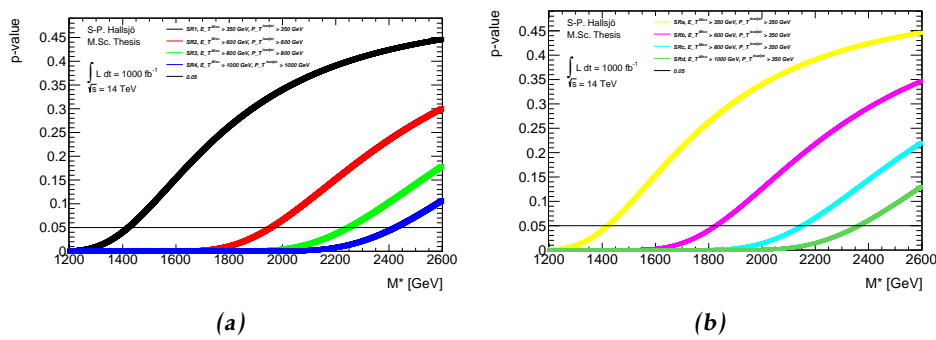


Figure 3.2: On a reco level error model 0.02.

Signal region	Mass suppression scale Truth data	Reco data
SR1	1425	1420
SR2	1960	1957
SR3	2249	2248
SR4	2423	2423
SRa	1425	1421
SRb	1900	1827
SRc	2197	2152
SRd	2389	2363

Table 3.7: Mass suppression scales in GeV given for the 0.02 error model.

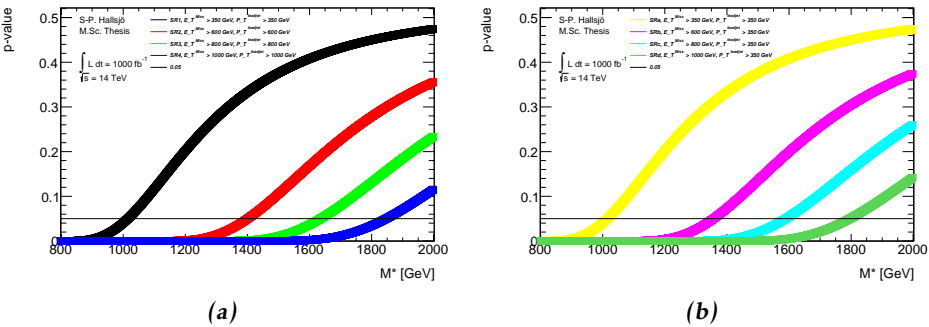


Figure 3.3: On a truth level error model 0.10.

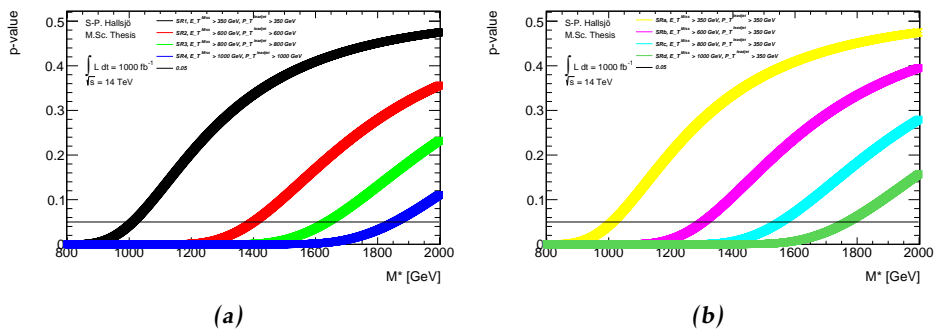


Figure 3.4: On a reco level error model 0.10.

3.4.4 Effect of pile-up on M^*

729 Hardly any effect. 10 % or in that vicinity.

Signal region	Mass suppression scale Truth data	Reco data
SR1	1015	1012
SR2	1400	1400
SR3	1636	1637
SR4	1846	1854
SRa	1015	1012
SRb	1356	1303
SRc	1589	1553
SRd	1796	1768

Table 3.8: Mass suppression scales in GeV given for the 0.10 error model.

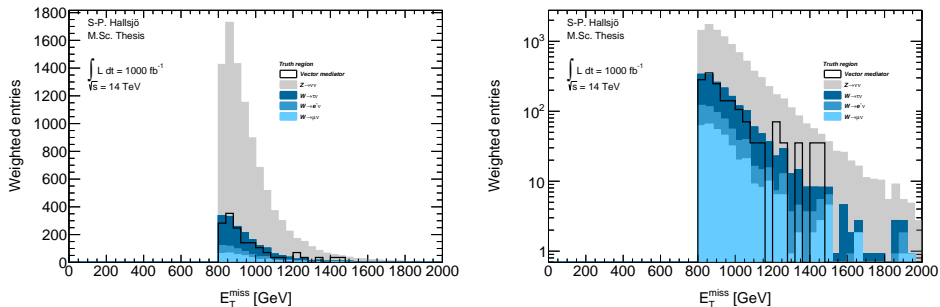
3.4.5 Previous results

732 10fb paper. Preliminary not that much better results for 1000fb-1 and 14TeV.

733 The whole discussion with Steven and David.

3.4.6 Limit on mediator mass

735 Are there previous results? Signal vs background plot in normal and log scale for
 736 one of the vector mediator models, to be able to evaluate all the different models
 737 the so called p-value was used in different signal regions. Below are two figures
 738 showing one of the vector mediator models in SR3.



(a) Signal on background plot for E_T^{miss} on
 739 reco level in SR3. (b) The same as a) with log scale on the y-axis

Figure 3.5: Signal on background plot to illustrate the a general plot.

739 To set a limit on the mediator mass the p-value was calculated in different sig-
 740 nal regions for the different signal models with different mediator mass. This
 741 resulted in the following plot:

742 3.4.7 Effect of pile-up on mediator mass

743 Check the different cases for reco and truth to see what happens.

744 **3.5 Discussion**

745 **3.5.1 Comparison to previous results**

746 **3.5.2 Effect of the high luminosity**

747 3.6 Conclusion**748 3.6.1 Limit on M^*** **749 3.6.2 Limit on mediator mass**

750

4

751

Results and Conclusions

752 **Disclaimer: This chapter not yet completed.**

753 4.1 Validation of smearing functions

754 Have some discussion.

755 Result they appear to work as expected, the reference paper was a bit unclear, I
756 leave my writing as a better reference.

757 **4.2 Signal to background ratio**

758 **4.2.1 Limit on M***

759 **4.2.2 Limit on mediator mass**

760 **4.3 Other selection criteria and observables**

761 **4.3.1 Limit on M***

762 **4.3.2 Limit on mediator mass**

763 **4.4 Mitigating the effect of the high luminosity**

764 **4.5 Recommendations to mitigate the effect of the 765 high luminosity**

766 Keep to a higher energy region, or signal region.

767 **4.6 Suggestions for future research**

768 With more time, search for new signal regions, the only solution now for the HL
769 is to go up in energy. Since none of the other parameters (eta,phi etc) seem to be
770 altered these can not be used. Is there something that has been overlooked?

771 Test the effect of pile-up for lower signal regions? See if the effect is as great as
772 predicted.

773 Explore other theoretical models for dark matter, other d operators etc. Models
774 that are based on Supersymmetry and not just effective theories.

775 Sätt av ett kort kapitel sist i rapporten till att avrunda och föreslå räkningar för
776 framtida utveckling av arbetet.

777 Saving as reference. test citing as: Here we cite Duck [29] [29].

778 If the above works, remember to edit myreferences.

Appendix

780

A

781

Datasets

782 A.1 Background processes

783 A.1.1 Validation

784 For the validation the following datasets were used, with a filter at generator level
785 at 450GeV for lead jet and MET.

786 mc12.157539.sherpa_ct10_znunupt280d4pd.v03 mc12.157534.sherpa_ct10_wenupt200d4pd.v03

788 mc12.157535.sherpa_ct10_wmunupt200d4pd.v03

789 mc12.157536.sherpa_ct10_wtaunupt200d4pd.v03

790 mc12.129160.pythia8_au2cteq6l1_perf_jf17d4pd.v03

791 mc12.129160.pythia8_au2cteq6l1_perf_jf17d4pd.v04

792 mc12.129170.pythia8_au2cteq6l1_gammajet_dp17d4pd.v04

793 They should be read as such: Monte Carlo version, dataset number, generator, ?
794 name.

795 A.1.2 Background to signals

796 The same as the above though now with the filter as indicated by their name. The
797 second znunu sample has been generated with and center of mass energy at 8
798 TeV.

799 mc12.157539.sherpa_ct10_znunupt280d4pd.v05

800 mc12.157539.8tev_sherpa_ct10_znunupt280d4pd.v05

801 mc12.157536.sherpa_ct10_wtaunupt200d4pd.v05

802 mc12.157534.sherpa_ct10_wenupt200d4pd.v05

803 mc12.157535.sherpa_ct10_wmunupt200d4pd.v05

804 A.2 Signals

805 A.2.1 Qcut

806 Qcut means that the original data has been split into different parts depending
 807 on the value of the lead jet pt.

808 A.2.2 D5 signal processes

```
809 mc12.188408.madgraphpythia_auet2bcteq6l1_d5_dm50_ms10000_
810 qcut200d4pd.v06
811 mc12.188409.madgraphpythia_auet2bcteq6l1_d5_dm50_ms10000_
812 qcut400d4pd.v06
813 mc12.188410.madgraphpythia_auet2bcteq6l1_d5_dm50_ms10000_
814 qcut600d4pd.v06

815 mc12.188411.madgraphpythia_auet2bcteq6l1_d5_dm400_ms10000_
816 qcut200d4pd.v06
817 mc12.188412.madgraphpythia_auet2bcteq6l1_d5_dm400_ms10000_
818 qcut400d4pd.v06
819 mc12.188413.madgraphpythia_auet2bcteq6l1_d5_dm400_ms10000_
820 qcut600d4pd.v06
```

821 All signals should be read as such: Monte Carlo version, dataset number, generator,
 822 ?, name of operator, dark matter mass, default mass suppression scale,
 823 qcut part. As discussed in reference

824

825 A.2.3 Light vector mediator processes

```
826 mc12.188414.madgraphpythia_auet2bcteq6l1_dmv_dm50_mm100_w3_
827 qcut200d4pd.v06
828 mc12.188422.madgraphpythia_auet2bcteq6l1_dmv_dm50_mm100_w3_
829 qcut400d4pd.v06
830 mc12.188430.madgraphpythia_auet2bcteq6l1_dmv_dm50_mm100_w3_
831 qcut600d4pd.v06

832 mc12.188415.madgraphpythia_auet2bcteq6l1_dmv_dm50_mm300_w3_
833 qcut200d4pd.v06
834 mc12.188423.madgraphpythia_auet2bcteq6l1_dmv_dm50_mm300_w3_
835 qcut400d4pd.v06
836 mc12.188431.madgraphpythia_auet2bcteq6l1_dmv_dm50_mm300_w3_
837 qcut600d4pd.v06

838 mc12.188416.madgraphpythia_auet2bcteq6l1_dmv_dm50_mm500_w3_
839 qcut200d4pd.v06
840 mc12.188424.madgraphpythia_auet2bcteq6l1_dmv_dm50_mm500_w3_
841 qcut400d4pd.v06
```

```
842 mc12.188432.madgraphpythia_auet2bcteq6l1_dmv_dm50_mm500_w3_
843 qcut600d4pd.v06

844 mc12.188417.madgraphpythia_auet2bcteq6l1_dmv_dm50_mm1000_w3_
845 qcut200d4pd.v06
846 mc12.188425.madgraphpythia_auet2bcteq6l1_dmv_dm50_mm1000_w3_
847 qcut400d4pd.v06
848 mc12.188433.madgraphpythia_auet2bcteq6l1_dmv_dm50_mm1000_w3_
849 qcut600d4pd.v06

850 mc12.188418.madgraphpythia_auet2bcteq6l1_dmv_dm50_mm3000_w3_
851 qcut200d4pd.v06
852 mc12.188426.madgraphpythia_auet2bcteq6l1_dmv_dm50_mm3000_w3_
853 qcut400d4pd.v06
854 mc12.188434.madgraphpythia_auet2bcteq6l1_dmv_dm50_mm3000_w3_
855 qcut600d4pd.v06

856 mc12.188419.madgraphpythia_auet2bcteq6l1_dmv_dm50_mm6000_w3_
857 qcut200d4pd.v06
858 mc12.188427.madgraphpythia_auet2bcteq6l1_dmv_dm50_mm6000_w3_
859 qcut400d4pd.v06
860 mc12.188435.madgraphpythia_auet2bcteq6l1_dmv_dm50_mm6000_w3_
861 qcut600d4pd.v06

862 mc12.188420.madgraphpythia_auet2bcteq6l1_dmv_dm50_mm10000_w3_
863 qcut200d4pd.v06
864 mc12.188428.madgraphpythia_auet2bcteq6l1_dmv_dm50_mm10000_w3_
865 qcut400d4pd.v06
866 mc12.188436.madgraphpythia_auet2bcteq6l1_dmv_dm50_mm10000_w3_
867 qcut600d4pd.v06

868 mc12.188421.madgraphpythia_auet2bcteq6l1_dmv_dm50_mm15000_w3_
869 qcut200d4pd.v06
870 mc12.188429.madgraphpythia_auet2bcteq6l1_dmv_dm50_mm15000_w3_
871 qcut400d4pd.v06
872 mc12.188437.madgraphpythia_auet2bcteq6l1_dmv_dm50_mm15000_w3_
873 qcut600d4pd.v06

874 mc12.188438.madgraphpythia_auet2bcteq6l1_dmv_dm50_mm100_w8pi_
875 qcut200d4pd.v06
876 mc12.188446.madgraphpythia_auet2bcteq6l1_dmv_dm50_mm100_w8pi_
877 qcut400d4pd.v06
878 mc12.188454.madgraphpythia_auet2bcteq6l1_dmv_dm50_mm100_w8pi_
879 qcut600d4pd.v06

880 mc12.188439.madgraphpythia_auet2bcteq6l1_dmv_dm50_mm300_w8pi_
881 qcut200d4pd.v06
882 mc12.188447.madgraphpythia_auet2bcteq6l1_dmv_dm50_mm300_w8pi_
883 qcut400d4pd.v06
```

884 mc12.188455.madgraphpythia_auet2bcteq6l1_dmv_dm50_mm300_w8pi_
885 qcut600d4pd.v06

886 mc12.188440.madgraphpythia_auet2bcteq6l1_dmv_dm50_mm500_w8pi_
887 qcut200d4pd.v06
888 mc12.188448.madgraphpythia_auet2bcteq6l1_dmv_dm50_mm500_w8pi_
889 qcut400d4pd.v06
890 mc12.188456.madgraphpythia_auet2bcteq6l1_dmv_dm50_mm500_w8pi_
891 qcut600d4pd.v06

892 mc12.188441.madgraphpythia_auet2bcteq6l1_dmv_dm50_mm1000_w8pi_
893 qcut200d4pd.v06
894 mc12.188449.madgraphpythia_auet2bcteq6l1_dmv_dm50_mm1000_w8pi_
895 qcut400d4pd.v06
896 mc12.188457.madgraphpythia_auet2bcteq6l1_dmv_dm50_mm1000_w8pi_
897 qcut600d4pd.v06

898 mc12.188442.madgraphpythia_auet2bcteq6l1_dmv_dm50_mm3000_w8pi_
899 qcut200d4pd.v06
900 mc12.188450.madgraphpythia_auet2bcteq6l1_dmv_dm50_mm3000_w8pi_
901 qcut400d4pd.v06
902 mc12.188458.madgraphpythia_auet2bcteq6l1_dmv_dm50_mm3000_w8pi_
903 qcut600d4pd.v06

904 mc12.188444.madgraphpythia_auet2bcteq6l1_dmv_dm50_mm10000_w8pi_
905 qcut200d4pd.v06
906 mc12.188452.madgraphpythia_auet2bcteq6l1_dmv_dm50_mm10000_w8pi_
907 qcut400d4pd.v06
908 mc12.188460.madgraphpythia_auet2bcteq6l1_dmv_dm50_mm10000_w8pi_
909 qcut600d4pd.v06

910 mc12.188445.madgraphpythia_auet2bcteq6l1_dmv_dm50_mm15000_w8pi_
911 qcut200d4pd.v06
912 mc12.188453.madgraphpythia_auet2bcteq6l1_dmv_dm50_mm15000_w8pi_
913 qcut400d4pd.v06
914 mc12.188461.madgraphpythia_auet2bcteq6l1_dmv_dm50_mm15000_w8pi_
915 qcut600d4pd.v06

916 mc12.188462.madgraphpythia_auet2bcteq6l1_dmv_dm400_mm500_w3_
917 qcut200d4pd.v06
918 mc12.188468.madgraphpythia_auet2bcteq6l1_dmv_dm400_mm500_w3_
919 qcut400d4pd.v06
920 mc12.188474.madgraphpythia_auet2bcteq6l1_dmv_dm400_mm500_w3_
921 qcut600d4pd.v06

922 mc12.188463.madgraphpythia_auet2bcteq6l1_dmv_dm400_mm1000_w3_
923 qcut200d4pd.v06
924 mc12.188469.madgraphpythia_auet2bcteq6l1_dmv_dm400_mm1000_w3_
925 qcut400d4pd.v06

```
926 mc12.188475.madgraphpythia_auet2bcteq6l1_dmv_dm400_mm1000_w3_
927 qcut600d4pd.v06
928 mc12.188464.madgraphpythia_auet2bcteq6l1_dmv_dm400_mm3000_w3_
929 qcut200d4pd.v06
930 mc12.188470.madgraphpythia_auet2bcteq6l1_dmv_dm400_mm3000_w3_
931 qcut400d4pd.v06
932 mc12.188476.madgraphpythia_auet2bcteq6l1_dmv_dm400_mm3000_w3_
933 qcut600d4pd.v06
934 mc12.188465.madgraphpythia_auet2bcteq6l1_dmv_dm400_mm6000_w3_
935 qcut200d4pd.v06
936 mc12.188471.madgraphpythia_auet2bcteq6l1_dmv_dm400_mm6000_w3_
937 qcut400d4pd.v06
938 mc12.188477.madgraphpythia_auet2bcteq6l1_dmv_dm400_mm6000_w3_
939 qcut600d4pd.v06
940 mc12.188466.madgraphpythia_auet2bcteq6l1_dmv_dm400_mm10000_w3_
941 qcut200d4pd.v06
942 mc12.188472.madgraphpythia_auet2bcteq6l1_dmv_dm400_mm10000_w3_
943 qcut400d4pd.v06
944 mc12.188478.madgraphpythia_auet2bcteq6l1_dmv_dm400_mm10000_w3_
945 qcut600d4pd.v06
946 mc12.188467.madgraphpythia_auet2bcteq6l1_dmv_dm400_mm15000_w3_
947 qcut200d4pd.v06
948 mc12.188473.madgraphpythia_auet2bcteq6l1_dmv_dm400_mm15000_w3_
949 qcut400d4pd.v06
950 mc12.188479.madgraphpythia_auet2bcteq6l1_dmv_dm400_mm15000_w3_
951 qcut600d4pd.v06
952 mc12.188480.madgraphpythia_auet2bcteq6l1_dmv_dm400_mm500_w8pi_
953 qcut200d4pd.v06
954 mc12.188486.madgraphpythia_auet2bcteq6l1_dmv_dm400_mm500_w8pi_
955 qcut400d4pd.v06
956 mc12.188492.madgraphpythia_auet2bcteq6l1_dmv_dm400_mm500_w8pi_
957 qcut600d4pd.v06
958 mc12.188481.madgraphpythia_auet2bcteq6l1_dmv_dm400_mm1000_w8pi_
959 qcut200d4pd.v06
960 mc12.188487.madgraphpythia_auet2bcteq6l1_dmv_dm400_mm1000_w8pi_
961 qcut400d4pd.v06
962 mc12.188493.madgraphpythia_auet2bcteq6l1_dmv_dm400_mm1000_w8pi_
963 qcut600d4pd.v06
964 mc12.188482.madgraphpythia_auet2bcteq6l1_dmv_dm400_mm3000_w8pi_
965 qcut200d4pd.v06
966 mc12.188488.madgraphpythia_auet2bcteq6l1_dmv_dm400_mm3000_w8pi_
967 qcut400d4pd.v06
```

```
968 mc12.188494.madgraphpythia_auet2bcteq6l1_dmv_dm400_mm3000_w8pi_
969 qcut600d4pd.v06
970 mc12.188483.madgraphpythia_auet2bcteq6l1_dmv_dm400_mm6000_w8pi_
971 qcut200d4pd.v06
972 mc12.188489.madgraphpythia_auet2bcteq6l1_dmv_dm400_mm6000_w8pi_
973 qcut400d4pd.v06
974 mc12.188495.madgraphpythia_auet2bcteq6l1_dmv_dm400_mm6000_w8pi_
975 qcut600d4pd.v06
976 mc12.188484.madgraphpythia_auet2bcteq6l1_dmv_dm400_mm10000_w8pi_
977 qcut200d4pd.v06
978 mc12.188490.madgraphpythia_auet2bcteq6l1_dmv_dm400_mm10000_w8pi_
979 qcut400d4pd.v06
980 mc12.188496.madgraphpythia_auet2bcteq6l1_dmv_dm400_mm10000_w8pi_
981 qcut600d4pd.v06
982 mc12.188485.madgraphpythia_auet2bcteq6l1_dmv_dm400_mm15000_w8pi_
983 qcut200d4pd.v06
984 mc12.188491.madgraphpythia_auet2bcteq6l1_dmv_dm400_mm15000_w8pi_
985 qcut400d4pd.v06
986 mc12.188497.madgraphpythia_auet2bcteq6l1_dmv_dm400_mm15000_w8pi_
987 qcut600d4pd.v06
```

Bibliography

- 990 [1] Collaboration ATLAS. Letter of Intent for the Phase-II Upgrade of the
991 ATLAS Experiment. Dec 2012. URL [https://cds.cern.ch/record/](https://cds.cern.ch/record/1502664/)
992 1502664/. Cited on pages 1, 17, 26, and 28.
- 993 [2] B.H. Bransden and C.J. Joachain. *Quantum mechanics*. Pearson Education,
994 second edition, 2000. Cited on page 3.
- 995 [3] Sven-Patrik Hallsjö. Covering the sphere with noncontextuality inequal-
996 ities. Bachelor's thesis, Linköping University, The Institute of Technol-
997 ogy, 2013. URL [http://urn.kb.se/resolve?urn=urn:nbn:se:liu:](http://urn.kb.se/resolve?urn=urn:nbn:se:liu:diva-103663)
998 diva-103663. Cited on page 3.
- 999 [4] A. Zee. *Quantum Field Theory in a Nutshell*. Princeton University Press,
1000 illustrated edition edition, March 2003. ISBN 0691010196. Cited on pages
1001 3, 6, and 7.
- 1002 [5] Herbert Goldstein, Charles P. Poole, and John L. Safko. *Classical Mechanics*
1003 (*3rd Edition*). Addison-Wesley, 3 edition, June 2001. ISBN 0201657023.
1004 Cited on page 3.
- 1005 [6] W. E. Burcham and M. Jobes. *Nuclear and Particle Physics*. Pearson edu-
1006 cation, second edition, 1995. Cited on page 4.
- 1007 [7] The ATLAS Collaboration. Observation of a new particle in the search
1008 for the Standard Model Higgs boson with the ATLAS detector at the LHC.
1009 *Phys. Lett. B*, 716(arXiv:1207.7214). CERN-PH-EP-2012-218):1–29. 39 p,
1010 Aug 2012. Cited on page 4.
- 1011 [8] Standard model of elementary particles. [http://en.wikipedia.org/](http://en.wikipedia.org/wiki/File:Standard_Model_of_Elementary_Particles.svg)
1012 [wiki/File:Standard_Model_of_Elementary_Particles.svg](http://en.wikipedia.org/wiki/File:Standard_Model_of_Elementary_Particles.svg),
1013 2014. Accessed: 2014-03-24. Cited on page 4.
- 1014 [9] G. Jungman, M. Kamionkowski, and K. Griest. Supersymmetric dark matter.
1015 *Physics Reports*, 267:195–373, March 1996. doi: 10.1016/0370-1573(95)
1016 00058-5. Cited on pages 4 and 5.

- 1017 [10] NASA. NASA's solar system exploration: the planets: orbits and
1018 physical characteristics. <https://solarsystem.nasa.gov/planets/>
1019 charchart.cfm, 2014. Accessed: 2014-03-21. Cited on page 6.
- 1020 [11] T. S. van Albada, J. N. Bahcall, K. Begeman, and R. Sancisi. Distribution
1021 of dark matter in the spiral galaxy NGC 3198. *Astrophysical Journal*, 295:
1022 305–313, August 1985. doi: 10.1086/163375. Cited on page 6.
- 1023 [12] Jessica Goodman, Masahiro Ibe, Arvind Rajaraman, William Shepherd,
1024 Tim M.P. Tait, et al. Constraints on Light Majorana dark Matter from Colliders.
1025 *Phys.Lett.*, B695:185–188, 2011. doi: 10.1016/j.physletb.2010.11.009.
1026 Cited on pages 5 and 7.
- 1027 [13] ATLAS Collaboration. Search for dark matter candidates and large extra di-
1028 mensions in events with a jet and missing transverse momentum with the at-
1029 las detector. *J. High Energy Phys.*, 04(arXiv:1210.4491. CERN-PH-EP-2012-
1030 210):075. 58 p, October 2012. URL [http://cds.cern.ch/record/](http://cds.cern.ch/record/1485031)
1031 1485031. Cited on pages 5, 8, and 9.
- 1032 [14] J. Goodman, M. Ibe, A. Rajaraman, W. Shepherd, T. M. P. Tait, and H.-B. Yu.
1033 Constraints on dark matter from colliders. *Phys.Rev.D82:116010,2010*, 82
1034 (11):116010, December 2010. doi: 10.1103/PhysRevD.82.116010. Cited on
1035 page 7.
- 1036 [15] ATLAS. Atlas luminosity public results. <https://twiki.cern.ch/twiki/bin/view/AtlasPublic/LuminosityPublicResults>, 2013.
1037 Accessed: 2014-03-06. Cited on page 10.
- 1039 [16] AC Team. The four main LHC experiments, Jun 1999. URL <http://cds.cern.ch/record/40525>. Cited on page 10.
- 1041 [17] Werner Herr and B Muratori. Concept of luminosity. 2006. URL <http://cds.cern.ch/record/941318/>. Cited on page 11.
- 1043 [18] The ATLAS Collaboration. The atlas experiment at the cern large hadron col-
1044 linder. *Journal of Instrumentation*, 3(08):S08003. 437 p, 2008. URL <https://cdsweb.cern.ch/record/1129811/>. Cited on pages 11 and 12.
- 1046 [19] Joao Pequenao. Computer generated image of the whole ATLAS detector,
1047 Mar 2008. URL <http://cds.cern.ch/record/1095924>. Cited on page
1048 12.
- 1049 [20] ATLAS Collaboration. Event display for one of the monojet candidates in
1050 the data. The event has a jet with $\text{pt} = 602 \text{ GeV}$ at $\eta = -1$ and $\phi =$
1051 2.6 , $\text{MET} = 523 \text{ GeV}$, and no additional jet with $\text{pt}_{\text{jet}} > 30 \text{ GeV}$ in the fi-
1052 nal state.. [https://atlas.web.cern.ch/Atlas/GROUPS/PHYSICS/](https://atlas.web.cern.ch/Atlas/GROUPS/PHYSICS/CONFNOTES/ATLAS-CONF-2011-096/fig_08.png)
1053 [CONFNOTES/ATLAS-CONF-2011-096/fig_08.png](https://atlas.web.cern.ch/Atlas/GROUPS/PHYSICS/CONFNOTES/ATLAS-CONF-2011-096/fig_08.png), 2011. Accessed:
1054 2014-03-28. Cited on page 13.
- 1055 [21] ATLAS Collaboration. Physics at a High-Luminosity LHC with ATLAS. Jul

- 1056 2013. URL <https://cds.cern.ch/record/1564937>. Cited on page
1057 15.
- 1058 [22] J. Alwall, M. Herquet, F. Maltoni, O. Mattelaer, and T. Stelzer. MadGraph
1059 5: going beyond. *Journal of High Energy Physics*, 6:128, June 2011. doi:
1060 10.1007/JHEP06(2011)128. Cited on page 15.
- 1061 [23] Torbjörn Sjöstrand, Stephen Mrenna, and Peter Skands. A brief introduc-
1062 tion to {PYTHIA} 8.1. *Computer Physics Communications*, 178(11):852 –
1063 867, 2008. ISSN 0010-4655. doi: [http://dx.doi.org/10.1016/j.cpc.2008.
1064 01.036](http://dx.doi.org/10.1016/j.cpc.2008.01.036). URL [http://www.sciencedirect.com/science/article/
1065 pii/S0010465508000441](http://www.sciencedirect.com/science/article/pii/S0010465508000441). Cited on page 15.
- 1066 [24] The ROOT Team. Root. <http://root.cern.ch/drupal/>, 2014. Ac-
1067 cessed: 2014-03-28. Cited on page 15.
- 1068 [25] S. Agostinelli, J. Allison, K. Amako, J. Apostolakis, H. Araujo, P. Arce,
1069 M. Asai, D. Axen, S. Banerjee, G. Barrand, F. Behner, L. Bellagamba,
1070 J. Boudreau, L. Broglia, A. Brunengo, H. Burkhardt, S. Chauvie, J. Chuma,
1071 R. Chytracek, G. Cooperman, G. Cosmo, P. Degtyarenko, A. Dell'Acqua,
1072 G. Depaola, D. Dietrich, R. Enami, A. Feliciello, C. Ferguson, H. Fe-
1073 sefeldt, G. Folger, F. Foppiano, A. Forti, S. Garelli, S. Giani, R. Gi-
1074 annitrapani, D. Gibin, J.J. Gómez Cadenas, I. González, G. Gracia
1075 Abril, G. Greeniaus, W. Greiner, V. Grichine, A. Grossheim, S. Guatelli,
1076 P. Gumligner, R. Hamatsu, K. Hashimoto, H. Hasui, A. Heikkinen,
1077 A. Howard, V. Ivanchenko, A. Johnson, F.W. Jones, J. Kallenbach, N. Kanaya,
1078 M. Kawabata, Y. Kawabata, M. Kawaguti, S. Kelner, P. Kent, A. Kimura,
1079 T. Kodama, R. Kokoulin, M. Kossov, H. Kurashige, E. Lamanna, T. Lampén,
1080 V. Lara, V. Lefebure, F. Lei, M. Liendl, W. Lockman, F. Longo, S. Magni,
1081 M. Maire, E. Medernach, K. Minamimoto, P. Mora de Freitas, Y. Morita,
1082 K. Murakami, M. Nagamatu, R. Nartallo, P. Nieminen, T. Nishimura, K. Oht-
1083 subo, M. Okamura, S. O'Neale, Y. Oohata, K. Paech, J. Perl, A. Pfeiffer,
1084 M.G. Pia, F. Ranjard, A. Rybin, S. Sadilov, E. Di Salvo, G. Santin, T. Sasaki,
1085 N. Savvas, Y. Sawada, S. Scherer, S. Sei, V. Sirotenko, D. Smith, N. Starkov,
1086 H. Stoecker, J. Sulkimo, M. Takahata, S. Tanaka, E. Tcherniaev, E. Safai
1087 Tehrani, M. Tropeano, P. Truscott, H. Uno, L. Urban, P. Urban, M. Verderi,
1088 A. Walkden, W. Wander, H. Weber, J.P. Wellisch, T. Wenaus, D.C. Williams,
1089 D. Wright, T. Yamada, H. Yoshida, and D. Zschiesche. Geant4—a sim-
1090 ulation toolkit. *Nuclear Instruments and Methods in Physics Research*
1091 *Section A: Accelerators, Spectrometers, Detectors and Associated Equip-
1092 ment*, 506(3):250 – 303, 2003. ISSN 0168-9002. doi: [http://dx.doi.org/
1093 10.1016/S0168-9002\(03\)01368-8](http://dx.doi.org/10.1016/S0168-9002(03)01368-8). URL <http://www.sciencedirect.com/science/article/pii/S0168900203013688>. Cited on page 17.
- 1094 [26] ATLAS Collaboration. Performance assumptions for an upgraded ATLAS
1095 detector at a High-Luminosity LHC. Mar 2013. URL <https://cds.cern.ch/record/1527529/>. Cited on pages 17, 20, 26, 27, and 28.
- 1096 [27] ATLAS Collaboration. Electron performance measurements with the ATLAS
1097

1099 detector using the 2010 LHC proton-proton collision data. *Eur. Phys. J. C*,
1100 72(arXiv:1110.3174. CERN-PH-EP-2011-117):1909. 45 p, Oct 2011. Com-
1101 ments: 33 pages plus author list (45 pages total), 24 figures, 12 tables, sub-
1102 mitted to Eur. Phys. J. C. Cited on pages 26 and 28.

1103 [28] ATLAS Collaboration. Search for New Phenomena in Monojet plus Missing
1104 Transverse Momentum Final States using 10fb-1 of pp Collisions at $\sqrt{s}=8$
1105 TeV with the ATLAS detector at the LHC. Nov 2012. URL [http://cds.
1106 cern.ch/record/1493486/](http://cds.cern.ch/record/1493486/). Cited on pages 32, 34, 35, and 36.

1107 [29] Donald Duck. The history of automatic control. *Duckburg Journal of Sci-
1108 ence*, 106(3):345–401, 2005. Cited on page 46.

1110 Upphovsrätt

1111 Detta dokument hålls tillgängligt på Internet — eller dess framtida ersättare —
 1112 under 25 år från publiceringsdatum under förutsättning att inga extraordinära
 1113 omständigheter uppstår.

1114 Tillgång till dokumentet innebär tillstånd för var och en att läsa, ladda ner,
 1115 skriva ut enstaka kopior för enskilt bruk och att använda det oförändrat för icke-
 1116 kommersiell forskning och för undervisning. Överföring av upphovsrätten vid
 1117 en senare tidpunkt kan inte upphäva detta tillstånd. All annan användning av
 1118 dokumentet kräver upphovsmannens medgivande. För att garantera äktheten,
 1119 säkerheten och tillgängligheten finns det lösningar av teknisk och administrativ
 1120 art.

1121 Upphovsmannens ideella rätt innehåller rätt att bli nämnd som upphovsman
 1122 i den omfattning som god sed kräver vid användning av dokumentet på ovan
 1123 beskrivna sätt samt skydd mot att dokumentet ändras eller presenteras i sådan
 1124 form eller i sådant sammanhang som är kränkande för upphovsmannens litterära
 1125 eller konstnärliga anseende eller egenart.

1126 För ytterligare information om Linköping University Electronic Press se för-
 1127 lagets hemsida <http://www.ep.liu.se/>

1128 Copyright

1129 The publishers will keep this document online on the Internet — or its possi-
 1130 ble replacement — for a period of 25 years from the date of publication barring
 1131 exceptional circumstances.

1132 The online availability of the document implies a permanent permission for
 1133 anyone to read, to download, to print out single copies for his/her own use and
 1134 to use it unchanged for any non-commercial research and educational purpose.
 1135 Subsequent transfers of copyright cannot revoke this permission. All other uses
 1136 of the document are conditional on the consent of the copyright owner. The
 1137 publisher has taken technical and administrative measures to assure authenticity,
 1138 security and accessibility.

1139 According to intellectual property law the author has the right to be men-
 1140 tioned when his/her work is accessed as described above and to be protected
 1141 against infringement.

1142 For additional information about the Linköping University Electronic Press
 1143 and its procedures for publication and for assurance of document integrity, please
 1144 refer to its www home page: <http://www.ep.liu.se/>